

# **YOLUX**

## **FIBER OPTICS EDUCATIONAL KIT**

---

**With Collaboration from  
Fiber Optics Group, Department of Physics  
Indian Institute of Technology Delhi**

---

### ***APPLICATION HANDBOOK***

*bipin behari dey & co*

# **Basic Experiments in Fiber Optics: A Laboratory Instruction Manual\***

\*Copyright©2004 by Fiber Optics Group, Physics Department, IIT Delhi. This manual is specifically written for the *YOLUX Fiber Optics Educational Kit*, which is manufactured by M/s Bipin Behari Dey & Co., Bhubaneswar; under license from FITT, IIT Delhi. The manual should not be copied and distributed. The authors will use the material in a future extended publication. While the authors have taken utmost care in describing correctly and appropriately the materials contained in this manual, they bear no responsibility for any damages resulting by the use of the contents of this manual.

## About the Manual

Fiber Optics has emerged as an important area in science and technology, and it is now entering the syllabus of many courses in engineering and physics at the graduate and post-graduate level. Most of these courses are presently offered as theory courses, and there is a need to supplement them with laboratory training. The *YOLUX Fiber Optic Educational Kit* has been developed to meet this requirement. Development of this kit has been a joint venture between the Fiber Optics Group at IIT Delhi and M/s Bipin Behari Dey & Co., Bhubaneswar. The kit is designed to give training in terms of handling of optical fibers, characterizing them and developing an understanding, which is required to embark on advanced work in fiber optics and related areas like optical fiber sensors.

In this manual, seven basic experiments have been described in detail, which can be performed with the YOLUX Fiber Optic Educational Kit supplied by M/s Bipin Behari Dey & Co., Bhubaneswar. The instrumentation for each experiment corresponds to the components and equipments provided with the YOLUX Kit. A unique feature of this Kit is the availability of two mechanical bread-boards for mounting the optical components – one at the input (launching) end, and the other at the output (detector) end. This provides flexibility in terms of isolating the detection setup at the output end from any stray light due to the source at the input end. While it will be very useful for the user to have a basic knowledge of fiber optics theory, it is not a prerequisite for performing the experiments. The references provided at the end of each experiment are specific to the experiment; for basic definitions, concepts and theory, the user may look into any standard book on Fiber Optics. We have also presented actual graphs and plots obtained in measurements carried out using components similar to the ones provided in the Kit, even though the plots are not ideal (as expected from theory) in some cases. We hope that it would help the students to appreciate some of the deviations expected in practice, when using a basic Kit like this.

In addition to the basic experiments described in this manual, depending on the level of students, the course instructor should be able to float several minor and major projects in the area of fiber optics. Some of them may, however, require additional components and equipments (which are not provided with the basic kit). Further, sophistication could be brought about into the measurement setups, which leads to higher accuracy and ease of measurement, by using for example, motorized scanners, highly sensitive detectors/power meter and a vibration-free table. All of these can be incorporated, if so desired, in a phased manner.

The experiments described in this manual form a part of the laboratory training of our students in the M.Tech programme on Optoelectronics and Optical Communication, which is jointly run by the Physics and Electrical Engineering departments in our Institute (IIT Delhi). These experiments have also been used in the training of participants in various summer and winter schools conducted at our Institute. We are grateful to all our colleagues who have contributed to the development of various experiments in our laboratory.

*Fiber Optics Group*  
Department of Physics  
I.I.T. Delhi, New Delhi – 16

## Contents

Expt.1 Fiber-end Preparation and Light Coupling .....	1
Expt.2 Numerical Aperture Measurement.....	9
Expt.3 Mode Field Diameter of a Single-Mode Fiber.....	15
Expt.4 Refractive Index Profile of a Multimode Fiber.....	21
Expt.5 Fiber-to-Fiber (Multimode) Splice Loss.....	28
Expt.6 Microbending Loss and Application in Sensing.....	34
Expt.7 Bend-induced Loss in a Single-Mode Fiber.....	41

# 1. Fiber-end Preparation and Light Coupling

---

## Aim

Preparation of fiber-end face and launching light into an optical fiber.

## Apparatus

Optical breadboard, laser diode, laser diode aligner, microscope objective (20X), microscope objective holder, xyz-translational stage, photodetector with multimeter, photo-detector holder, two fiber chucks, two post-bases and 3 posts, 2 m length (approx.) of a single-mode as well as a multimode fiber, razor blade, fiber cutter, and index matching liquid.

### 1.1 Fiber-end preparation

The very first step that one must follow before making any measurement/application involving use of optical fibers is to obtain optically-flat fiber end-faces perpendicular to the axis of the fiber, in order to ensure a good coupling efficiency between a light source and a fiber. This process is referred to as 'fiber-end preparation'. The acceptable optical quality of the end-finish and tolerance allowable with respect to end-face angle (i.e. the angle between the fiber end-face and the plane perpendicular to the axis of the fiber), however, depend on particular measurement/application. Conventional grinding and polishing techniques can indeed produce a very smooth end face that is perpendicular to the fiber axis. In this process, the test fiber is bonded with an optical epoxy within a glass/fused silica capillary tube, and the extreme ends of the combined structure is ground and polished together. However, this method is quite tedious and time-consuming and is rarely used in practice except in very special cases, where one requires an extremely high quality fiber end-face e.g. in fiber-based Fabry-Perot resonators, and high-quality end-faces of connectorized fiber pigtails and patch cords.

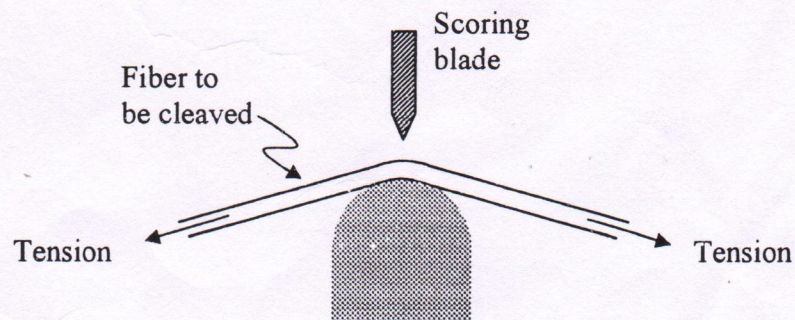


**Fig. 1.1** Controlled-fracture of an optical fiber for its end-preparation through bend, score and break technique.

One can produce a reasonably smooth and perpendicular end face by means of a controlled-fracture technique, which is based on 'bend-score-and-break' method for cleaving fibers, and is sufficient for most experiments. In this method, after removal of the outer protective jacket, the fiber to be cleaved is first scored with a scribe to initiate a crack at its surface. The scribe, which is required to be harder than silica glass, is typically a diamond-edged or a tungsten carbide blade. The fiber is then bent over a curved surface under tension, as shown in Fig. 1.1. For a silica fiber of 125  $\mu\text{m}$  overall diameter, the radius of curvature of the surface is about 57 mm. This action produces a stress distribution across the fiber cross-section. The maximum stress occurs at the scratch point so that a crack starts to propagate through the fiber, which eventually leads to cleaving of the fiber when the fiber is gently pulled apart by hands[1].

A variety of fiber cutting tools based on this methodology have been developed and are being used extensively. However, a controlled-fracture method requires careful control of the curvature of the fiber and the amount of the tension required to induce cleavage. If the stress distribution across the fiber is not properly controlled, the fracture propagating across the fiber can fork into several cracks. This forking produces surface defects such as a "lip" or "hackle" on the fiber end, as shown in the Fig. 1.2.

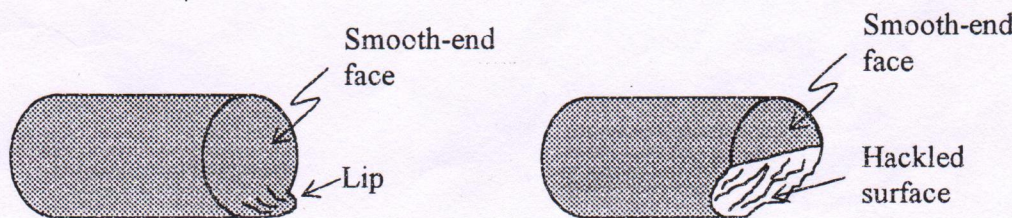


**Fig. 1.2 Two examples of improperly cleaved fiber ends.**

In the absence of a commercial tool, one can obtain, with some experience, good quality fiber end-faces by following the procedure described below:

1. Remove the outer protective jacket of the fiber over a few centimeters length near the fiber end. Depending on the material used, the protective jacket may be removed using a suitable chemical solvent (e.g. dichloro-ethylene) or may be simply peeled off using a sharp razor blade.
2. The bare fiber is held by the thumb and the middle finger, and is positioned on the curved surface near the tip of the fore-finger, the palm facing upwards (see Fig. 1.3).
3. A small crack is then initiated by gently scoring on the surface of the fiber (which is positioned on the fore-finger) with a steady hand, in a direction perpendicular to the fiber length.
4. Now, without changing the grip on the fiber, the fiber length beyond the crack is gently pulled apart along the axis of the fiber.

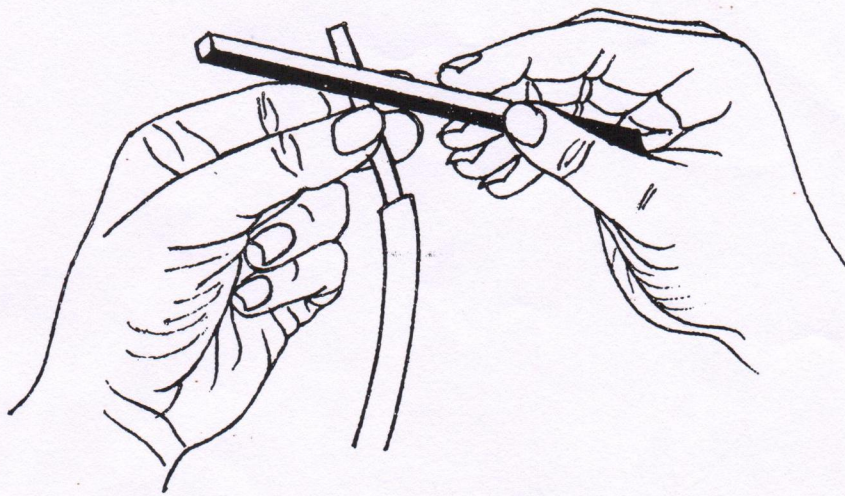


**Figure 1.3** The correct way of holding the fiber while scribing the surface for end preparation.

As a result, the fiber is likely to cleave with a good end-face. If this does not happen, then repeat the above procedure by initiating a fresh crack, at a slightly different position on the fiber.

A quick and effective assessment of the quality of the cleaved fiber end-face can be made by launching light from the laser diode into the fiber at the farther end, and observing the output light on a screen placed a few centimeters away. Poor cleavage is revealed by the presence of scattered light in the form of a 'comet tail' stretching away from an otherwise circular shaped far-field spot on the screen. Further, if the fiber is poorly cleaved, the fiber-end can be seen glowing even when viewed from the sides, as a result of scattering [2]. In the case of single-mode fibers, one can also observe one or two bright and dark rings circumscribing the central bright spot on a screen placed near the fiber end. The fiber-end will be good enough for most measurements if each of these rings are distinct, and appear to have uniform illumination all over the circumference.

## **1.2 Launching light into an optical fiber**

The most common method of launching light into an optical fiber in a laboratory experiment involves use of a suitable microscope objective (MO) in between the source and the fiber. The choice of the MO depends on the types of source and the fiber under consideration. The two important parameters of a MO are the *magnification* and the *numerical aperture* (NA), usually inscribed on the metallic case of the MO. Normal MOs typically comprise of a combination of 3 lenses, while MOs with special imaging requirements may have a number of lenses forming a complex lens system. However, for our purpose, MO is nothing but a good quality lens to focus light (with minimum aberrations) from a collimated source into a fine spot at its focus, where the fiber-end is required to be approximately positioned in order to couple light into the fiber.

### 1.2.1 MO as a lens

Consider the normal incidence of a collimated beam of light on the input aperture of the MO, completely filling its aperture (see Fig. 1.4). If  $\theta_a$  is the semi-angle of the focussed cone of light (on

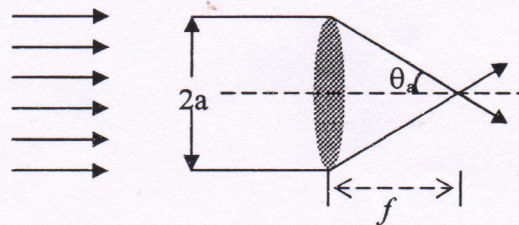


**Fig. 1.4** A lens representing a MO of focal length  $f$  and numerical aperture  $\sin \theta_a$ .

the other side), then the numerical aperture (NA), by definition, is given by the value of  $a/f (= \tan \theta_a \approx \sin \theta_a)$ . Thus  $\theta_a$  represents the maximum angle that the rays subtend with the axis of the MO at its focus. From Fig. 1.4, it is obvious that, for a given diameter of the front-end lens of the MO, larger NA implies smaller focal length and vice versa. This is an important observation for the user of a microscope objective for coupling light into an optical fiber, because the fiber-end should be placed in the close vicinity of the focus for achieving maximum light coupling into the fiber. The actual focal length of a MO corresponding to a given NA varies from one manufacturer to another and also upon the type of MO and the material of the lenses used. However, just to give the details of the MOs, which could be used in the experiments listed in this book, we have listed a few typical parameters [3]:

Magnification	NA	focal length
10X	0.25	~10 mm
20X	0.40	~4 mm
40X	0.65	~2 mm

### 1.2.2 Aligning the source and the MO

In order to launch light into an optical fiber using an MO, the first step involves aligning the MO with the source (laser diode); this is an important requirement for coupling maximum possible light



**Fig. 1.5** The spot of light at the output of MO, which shows the circular spot due to the MO and the intensely bright spot due to the laser diode.

into the fiber. The laser diode is mounted horizontally on the aligner having provision for height and tilt adjustments. The MO is mounted on the microscope objective holder in front of the laser diode at the same height as the source. The laser diode aligner and microscope objective holder, provided with the Educational Kit, are manufactured in such a way that if the axis of laser diode is exactly horizontal, it coincides with the axis of MO, when fixed on the aligner. So, one needs to carefully mount the source on the source aligner with the help of screws provided on the aligner.

When light from the laser diode is incident on the input aperture of the MO, the output spot of light, on the other side of the MO, contains a circular spot due to the MO and an intensely bright spot elliptical in shape due to the elliptical spot of the laser diode. The laser diode is adjusted with the help of screws provided on the aligner so that the center of the intensely bright elliptical output spot of the laser diode coincides with the circular spot of the MO as shown in Figure 1.5. This ensures a good alignment of the laser diode with the MO.

A tungsten halogen lamp is the most commonly used ‘white-light source’ in measurements involving multimode fibers such as numerical aperture measurement and the near-field scanning technique to determine the refractive index profile. The lamp is usually housed in a ventilated (or air-cooled) metallic chamber fitted with a variable aperture at the output. For a given MO, the launch NA can be controlled using the variable aperture. The MO can be aligned with the source by observing the intensity distribution of the focused light on a screen placed at a suitable distance in front of the MO, i.e. the intensity distribution in a cross-section of the cone of light emanating from the MO. When this circular cross-section appears uniformly bright about the center, and is concentric with the circular ‘image’ of the output aperture of the MO (which also appears on the screen as a weakly illuminated circular disc), reasonably good alignment is achieved.

### **1.2.3 Coupling light into the fiber**

After preparing good quality fiber ends, the fiber is firmly clamped over the fiber chucks with magnets, such that only a small length (not more than 5 mm) of the free fiber end projects out of the chuck. The fiber chuck is then mounted on a XYZ-stack, i.e. a stack of micropositioners that can provide translational movement along the three perpendicular directions - X, Y, and Z. With the help of the translational movement screws, the fiber end is precisely positioned near the focus of the

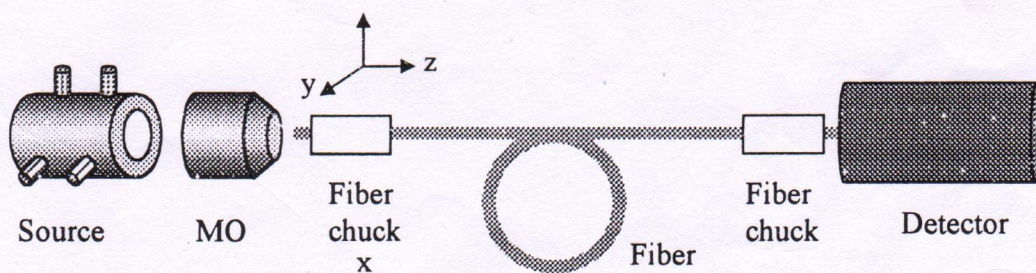


**Fig. 1.6 Experimental setup for launching light from a laser diode into an optical fiber using an MO.**

MO to achieve maximum light coupling into the fiber. A schematic of such a coupling arrangement is shown in Fig. 1.6. In order to obtain a stable light-coupling arrangement, it is essential to avoid any possible relative motion (say, due to vibrations) between the MO and the fiber end. The following step-by-step procedure would help in achieving maximum light coupling into the fiber:

1. Place the XYZ-stack such that the fiber chuck is aligned with the MO. Adjust further to bring the fiber-end near to the focus of the MO.
2. Manipulate the X and Y (transverse) stages to get some light at the output end of the fiber. Maximize the output at this (longitudinal) position Z. Usually the coupling will be best, when the fiber end is placed within the focus of the MO.
3. Now, move the fiber end by a small distance in the +ve z-direction (with respect to its position achieved in the step 2), and again maximize the output power using X and Y stages. If this maximum is lower than the previous maximum (at step no. 2), then move the fiber in the negative z-direction and adjust for the maximum output power.
4. The process is repeated till the optimum fiber position corresponding to the best coupling efficiency is achieved.

### **1.3 Cladding mode stripping**

Cladding modes may be defined as modes guided along the length of the fiber by the cladding-jacket or the cladding-air interface, in analogy to the definition of the guided modes. Here 'jacket'

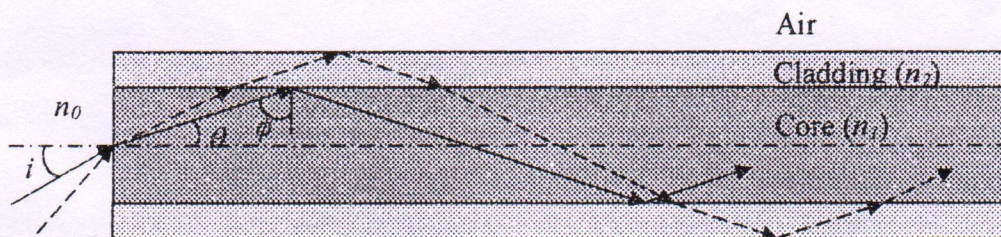


**Fig. 1.7 Ray diagram illustrating the propagation of guided and cladding modes in an optical fiber**

refers to the outer protective plastic/polymer layer, with which a bare fiber is coated immediately after it is drawn into a fiber from its preform. When light is launched into an optical fiber, the effective launch NA of the MO is usually chosen to be higher than the NA of the fiber. If the material of the jacket is of a lower refractive index than that of the cladding, then some of the rays transmitted through the core-cladding interface can satisfy the condition for total internal reflection at the cladding-jacket interface, giving rise to the excitation of cladding modes. Figure 1.7 illustrates this situation through the ray-optics. Note that the rays reflected by the cladding-air interface represent even higher NA than those, which form the core modes and therefore, the bare fiber will also support cladding modes.

Since the jacket comprises of a coating of rapidly condensed fluid, the cladding-jacket interface is usually not uniform; further, the material of the jacket is relatively lossy. Thus the behaviors of cladding-modes are quite unpredictable, and they attenuate rapidly as they propagate along the fiber. However, in many experiments on the characterization of an optical fiber, one uses a short length of the fiber, and therefore cladding modes may carry a significant amount of optical power to

the detector, resulting in spurious signals. Thus, it becomes necessary, virtually in all experiments, to eliminate the cladding modes before they reach the detector.

A simple method of eliminating, or 'stripping off' the cladding modes involves use of applying an index-matching liquid such as glycerin or liquid paraffin over a few centimeters length of the bare fiber near both the input and the output ends of the fiber. The liquid should, however, not come in contact with the fiber end-faces. The refractive index of the liquid used should be slightly greater than or equal to that of the cladding, so that the rays transmitted through the core-cladding interface do not satisfy the condition for total internal reflection at the cladding-liquid interface. Thus, the rays entering the cladding will eventually leak out within a few centimeters length of the fiber.

#### **1.4 Coupling of light from the fiber to a photo detector**

Light from the output end of a fiber comes out in the form of a cone of semi-angle  $\theta$ , which is determined by the numerical aperture of the fiber. In order to measure the output power in the visible and near infra-red region; a suitable detector such as Si photodiode is used. The fiber-to-detector light-coupling mechanism employed depends on the active area of the detector. In fiber characterization experiments, usually a *large area detector* (i.e. area  $\sim 1 \text{ cm}^2$ ) is used. In this case, the fiber output end is placed in front of the detector, such that the output from the fiber fills about 70 % of the detector's active area, i.e. the output light-spot lies well within the active area of the detector. This insures that the detector is not saturated locally and any variations in detector-surface response are averaged out. If the entire light spot lies within the active area, then the detector output is a measure of the total optical power incident on the detector. In the Educational Kit, the detector is connected to a multimeter, which shows photovoltage that is proportional to the photocurrent generated by the detector. Since the photocurrent is proportional to the optical power incident on the detector, the voltmeter reading is proportional to the optical power. Thus one can measure the intensity distribution across an optical beam using this arrangement. The voltmeter readings typically vary from 10s of microvolts to 10s of millivolts, depending on the incident power.

The above situation corresponds to measurement of the total output power. In situations where the intensity distribution at the output is to be measured, a pinhole-masked large area detector is usually employed to scan the output light spot along a diameter. Now the detector output is proportional to the intensity of light at the position of the pinhole, and therefore the scan represents the intensity distribution.

#### **1.5 Laser diode as an optical source**

The principal light sources used for fiber optic communications applications are *semiconductor laser diodes* (also referred to as injection laser diodes) and *light emitting diodes* (LED). These devices are suitable for fiber transmission systems because they have adequate output power for a wide range of applications and their optical power output can be directly modulated by varying the input current to the device; they have a high efficiency and their dimensional characteristics are compatible with those of the optical fiber.

The major difference between LEDs and laser diodes is that the optical output from an LED is incoherent, whereas that from a laser diode is coherent. In a coherent source the optical energy is

produced in an optical resonant cavity by the phenomenon of stimulated emission. The optical beam released from such a cavity usually has a very high degree of coherence, and is also very directional. The present day lasers are based on *double heterostructures* in which a thin active layer of a semiconductor with a lower bandgap is sandwiched between two larger bandgap semiconductors. The refractive index of the semiconductor decreases with increase in the bandgap. Thus the refractive index of the central active layer is higher than the two surrounding regions. Such a refractive index profile can confine the emitted optical radiation to the active region by the mechanism of waveguidance, which occurs due to total internal reflection taking place at the boundaries [4]. Although the active region is very thin, this doesn't lead to a narrow slit-like output beam; there is substantial diffraction of the output at the interface with air. Thus the output beam from a laser diode is not a narrowly defined spot or even a strip. It rapidly becomes a broad beam, and in order for light not to be wasted a collecting lens should be placed immediately adjacent to the output. One can use collimating lenses to obtain a well-collimated output laser beam. The laser source used in the Educational Kit is a semiconductor laser fitted with an external collimating lens.

## References

1. D. Gloge, P. W. Smith, D. L. Bisbee and E. L. Chinnock, "Optical Fiber-end Preparation for Low Loss Splices", *Bell Syst. Tech. J.*, vol. 52, pp. 1579-1588 (1973).
2. B.P. Pal, K. Thyagarajan and A. Kumar, "Characterization of Optical Fibers for Telecommunication and Sensors - Part I: Multimode Fibers" in *Fundamentals of Fiber Optics in Telecommunication and Sensor Systems*, B.P. Pal (Ed.), Wiley Eastern Ltd., New Delhi (1992).
3. A. K. Ghatak and M. R. Shenoy (Ed.), *Fiber Optics Through Experiments*, Viva Books P. Ltd., New Delhi, (1994).
4. A. K. Ghatak and K. Thyagarajan, *Introduction to Fiber Optics*, Cambridge University Press, Cambridge (1998).

## 2.Numerical Aperture Measurement

### Aim

To determine the numerical aperture (NA) of a given multimode fiber from the measurements on the far-field of the fiber.

### Apparatus

Bread board, tungsten halogen lamp (THL), microscope objective (20X), microscope objective holder, xyz-translational stage, pin-hole photodetector with multimeter, photodetector holder, rotation stage, two fiber chucks, two post bases and 3 posts, approx. 2 m length of a multimode fiber, razor blade, fiber cutter, index matching liquid.

### Theory

The extremely important parameter, which determines the maximum acceptance angle

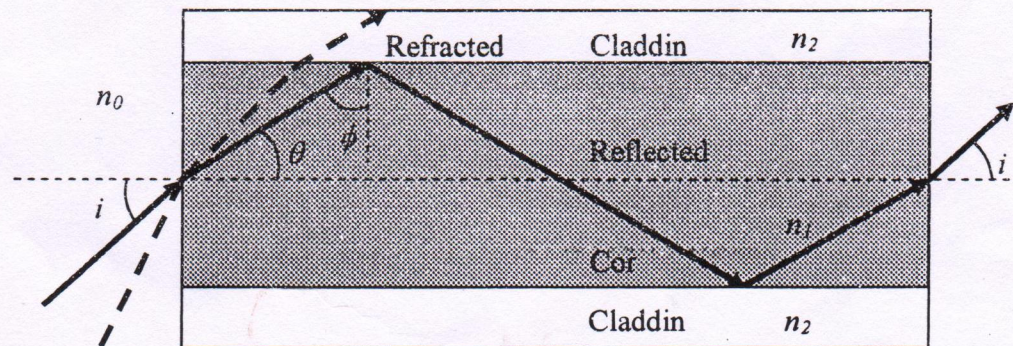


**Fig. 2.1** A meridional ray entering a step index optical fiber at an angle  $i < i_m$  gets guided through the fiber, and comes out at the same angle  $i$  from the output end of the fiber. Rays incident at angles  $> i_m$  will get refracted into the cladding, eventually losing all their energy in the cladding.

upto which the rays which are incident at the input face of a fiber and are to be guided through an optical fiber, is referred to as numerical aperture of the fiber and is given by [2]

$$NA = \sin i_m = \left( n_1^2 - n_2^2 \right)^{1/2} \quad (2.1)$$

where  $n_1$  and  $n_2$  are the refractive indices of the core and the cladding, respectively. Figure 2.1 shows the geometrical ray path of a particular meridional ray in a step index

multimode fiber. The light ray enters the fiber core from a medium of refractive index  $n_0$  at an angle  $i$  with respect to the fiber axis and strikes the core cladding interface at an angle  $\phi$  with respect to the normal to the interface. If  $\phi$  is greater than the critical angle  $\phi_c (= \sin^{-1}(n_2/n_1))$ , the ray gets totally internally reflected and because of the symmetry of the structure the same ray suffers repeated total internal reflections as shown in the Fig. 2.1. All such meridional rays follow zigzag paths along the fiber core, passing through the axis of the fiber after each reflection.

The semi angle  $i_m$  of the acceptance cone for a step-index fiber is determined by this critical angle  $\phi_c$ . Thus, if a ray is launched into the fiber at an angle  $\theta < i_m$ , it will be guided through the fiber, whereas a ray launched into the fiber at an angle  $\theta > i_m$  undergoes only partial reflection at the core cladding interface and will eventually radiate completely into the cladding.

The NA of the fiber is usually determined by measuring the angular dependance of the far field of the fiber. The far-field of the fiber represents the field distribution at any distance  $z \gg (2a)^2/\lambda$  where  $a$  is the core radius of the fiber and  $\lambda$  is the operating wavelength. In a short length of straight fiber, ideally, a ray launched at an angle  $i$  at the input end should come out at the same angle  $i$  from the output end as shown in Fig 2.1. Therefore far-field at the output end will also appear as a cone of semi-angle  $i_m$  emanating from the fiber end. It is then simpler to make measurements on this far-field to determine the NA of the fiber.

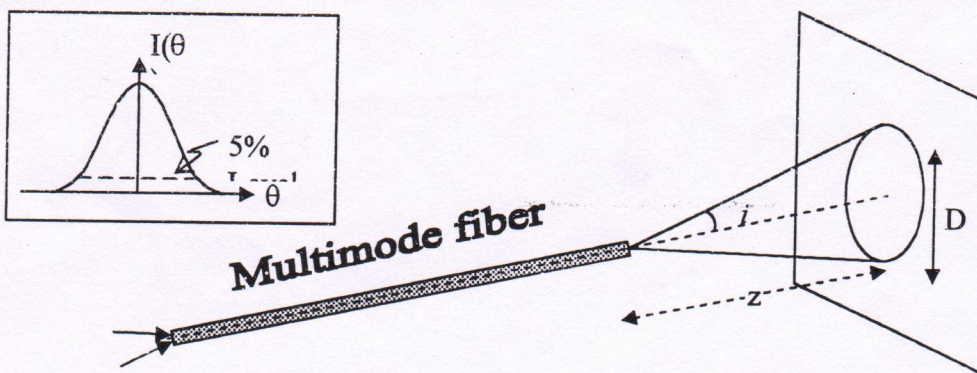


**Fig. 2.2** Measurement of the diameter  $D$  of the spot, corresponding to the angle  $i$  at which the intensity drops down to 5% of the maximum value (at  $i=0$ ), on the screen placed at a distance  $z$  in the far-field from the output end of a multimode fiber can be used to estimate the NA of the fiber. Inset shows the far-field pattern and the 5% level.

The NA of a fiber is determined by measuring the angular dependance of the far field. The semi-angle corresponding to the 5% level of the far-field intensity maximum is denoted as the acceptance angle. This angle is usually small and hence, in the absence of a suitable arrangement for the measurement of the angular dependance of the far-field

intensity, one may use direct visual estimation. In direct visual estimation, one carries out the measurements on the far-field projected on a plane perpendicular to the fiber axis by determining the diameter corresponding to the 5% intensity level (see Fig 2.2). The numerical aperture is then estimated using the following relation

$$NA = \sin i_m = \sin[\tan^{-1}(D/2z)] \quad (2.2)$$

### Procedure

Figure 2.3 shows the experimental set-up for the measurement of the numerical aperture of a multimode fiber. For this, one has to follow the following procedures step by step:

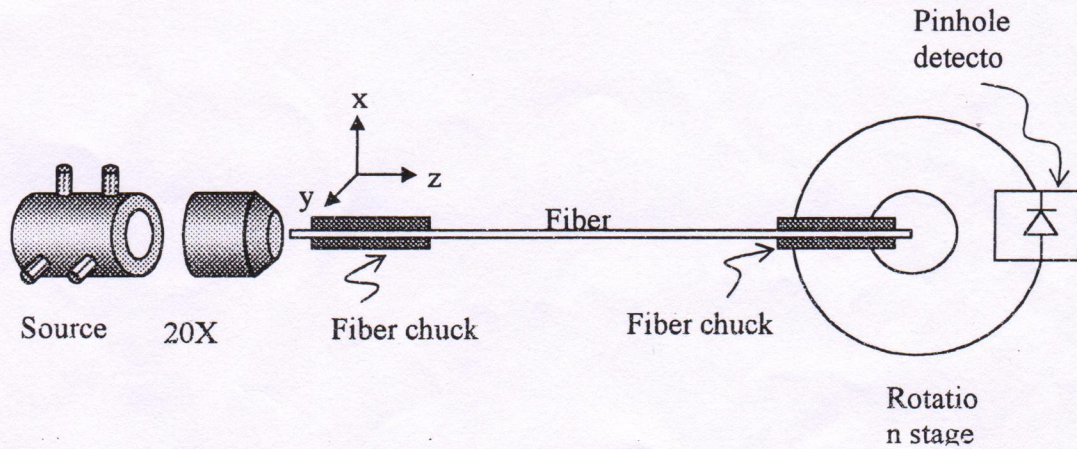


**Fig. 2.3** Experimental setup for scanning the far-field intensity distribution of a fiber.

1. Mount the THL and adjust with the help of the aligning screws to align it with the microscope objective.
2. Fiber ends are prepared so that it has well-cleaved flat ends. The cladding modes are removed by applying an index matching liquid (e.g. liquid paraffin) over a few centimeters of the bare fiber, near both the input and the output ends (after the removal of protective plastic jacket) and then clamped over the fiber chucks with magnets.
3. The output end of the fiber is clamped over a post base in such a way that the tip of the fiber is positioned on the axis of rotation of the rotational stage, which passes through the center of cross wire put over the mirror, fixed on the rotational stage. To do so, one has to continuously look the image of output end of the fiber on the mirror.
4. Light is launched into the fiber from the THL using a 20X-microscope objective.
5. A pinhole photodetector is mounted on the rotational stage and the height of the fiber tip is so adjusted that the pinhole is at the same horizontal level as that of the fiber end.
6. Now, without disturbing the input coupling, far-field (circular) spot of the fiber is scanned in suitable steps (say, in steps of  $0.2^\circ$ ), and at each angular position, the detected power recorded by the detector is noted down.

7. Plot of the detector reading versus the angular position of the detector represents the far-field intensity distribution. From this plot the half angle  $i_m$  corresponding to 5 % of the maximum intensity level is determined.
8. Numerical aperture of the fiber is given by

$$NA = \sin i_m \quad (2.3)$$

Figure 2.2 shows a schematic for direct visual estimation of the NA. Several concentric circles of increasing radii are drawn on a small screen placed normal to the fiber axis. The screen is positioned in the far-field in such a way that a line extending the axis of the fiber on the screen from its output end would have passed through the center of these circles, drawn on the screen. The fiber end, which is mounted on a XYZ-stack, is moved slightly towards or away from the screen so that the emerging light spot fills completely one of the circles, lets say of diameter  $D$  (which is measured accurately). The NA is calculated using Eq. (2.2).

## Observations

### 1) Visual Method:

Least count of Meter Scale =

S. No.	Radius of circle (cm) $D/2$	Distance from the fiber, $z$ (cm)	$NA = \sin i_m$ $= \sin[\tan^{-1}(D/2z)]$

### 2) Scanning Method:

Least count of the rotation stage =

S. No.	Reading on the rotation stage (in degrees)	Power meter reading ( $\mu W$ )

## Result

An experimentally measured angular distribution of the far-field (as measured by photodetector) for a given multimode fiber ( $NA = 0.26$ ) is shown in Fig. 2.4, where the filled squares show experimentally measured values. The horizontal line drawn in the

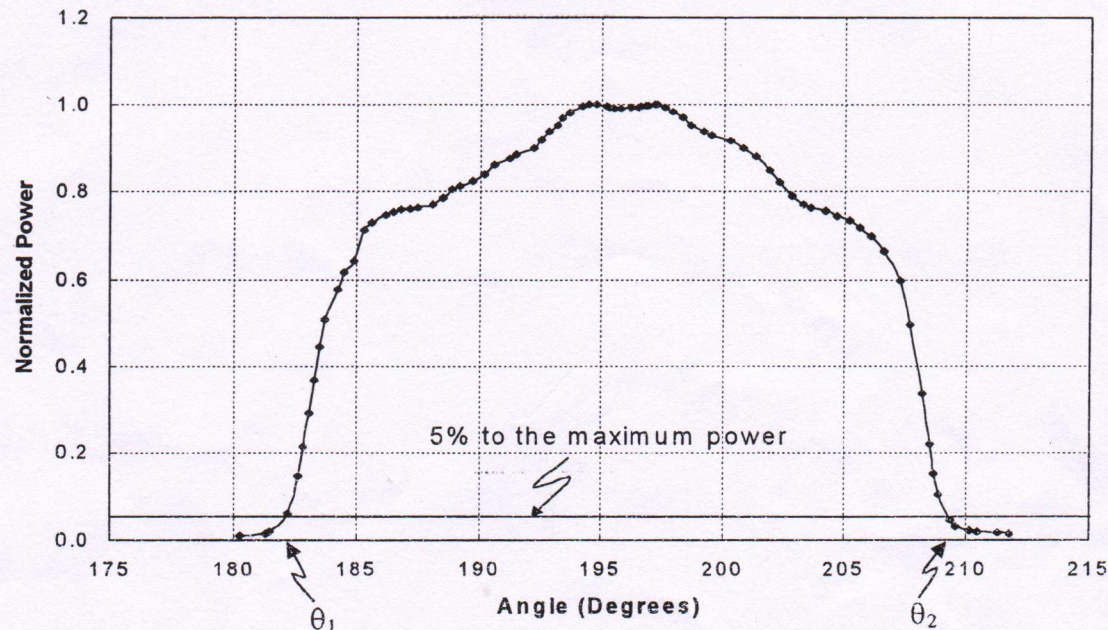


Fig. 2.4 Experimentally observed far-field pattern of a given step index multimode fiber

plot shows the level at which the intensity drops down to 5% of the maximum output power. This line intersects with the plot at two angles, which are marked as  $\theta_1$  and  $\theta_2$  in Fig. 2.4.

The values of  $\theta_1$  and  $\theta_2$ , as can be read from the above figure, are  $182.1^\circ$  and  $209.3^\circ$  respectively. The angle  $i_m [= (\theta_2 - \theta_1)/2]$ , can be calculated from these two values which comes out to be  $13.7^\circ$ . The numerical aperture of the given multimode fiber is then calculated using Eq. (2.3) which is equal to 0.24 and closely agrees with the value supplied by the manufacturer. At the same time, the direct visual estimation method yields the numerical aperture as equal to 0.20 for the same fiber, which is less than what we have measured using the far-field technique. This shows that the far-field technique for the determination of numerical aperture is more accurate in comparison to the direct visual estimation method and the result obtained by this method is in good agreement with the actual value of the NA of the fiber.

## **Comments**

In a multimode fiber, different mode groups suffer different attenuation rates, which is referred to as differential mode attenuation (DMA). NA measured by equation (2.3) is generally less than that estimated from equation (2.1) due to DMA. In addition, NA is critically dependent on the excitation conditions. To ensure that all the guided modes are excited in a multimode fiber, an "overfill launch" is applied at the input end i.e. one uses a microscope objective of NA higher than that of the fiber for launching light into the fiber. This results in the excitation of the cladding modes and the radiation modes, which quickly lose power as they propagate along the fiber. Further the higher order guided modes, which have a significant fraction of the total guided power in the cladding, attenuate faster as compared to the lower order modes. Therefore, in general, the modal power distribution within the fiber attains a steady state only after propagating some distance ( $\approx$  a few tens of meters) along the fiber length of the fiber. Consequently, the measured NA of a multimode fiber exhibits length dependence over relatively short length of the fiber.

The analyses discussed under the theory section are based on meridional rays. However, a greater power loss arises when skew rays are included in the analyses, since many of the skew rays that geometric optics predicts are trapped in the fiber are actually leaky rays. These leaky rays are only partially confined to the core of the circular optical fiber and attenuate as the light travels along the fiber. Thus, a detailed inclusion of skew rays will change the expression of the light acceptance ability (NA) of the fiber.

Although this method appears to be quite simple and straightforward, extreme care should be taken to ensure the following points at the time of experiment:

1. The fiber end faces must be of good quality.
2. Cladding-mode strippers must be used.
3. The output end of the fiber must be positioned in such a way that the output end tip of the fiber is concentric with center of the rotation stage.

## **References**

1. B. P. Pal, K. Thyagarajan and A. Kumar, "Characterization of Optical Fibers for Telecommunication and Sensors-Part I: Multimode Fibers" in *Fundamental of Fiber Optics in Telecommunication and Sensor Systems*, B. P. Pal (Ed), Wiley Eastern Ltd., New Delhi (1992).
2. A. K. Ghatak and K. Thyagarajan, *Introduction to Fiber Optics*, Cambridge University Press, Cambridge (1998).
3. A. K. Ghatak and M. R. Shenoy, *Fiber Optics Through Experiments*, Viva Books Pvt. Ltd., New Delhi (1994).
4. A. W. Snyder and J. D. Love, *Optical Waveguide Theory*, Routledge Chapman and Hall, New York, (1984).

### **3. Mode Field Diameter of a Single-Mode Fiber**

---

#### **Aim**

To determine the mode field diameter (MFD) of the fundamental mode in a given single-mode fiber (SMF) by a measurement of its far-field.

#### **Apparatus**

Bread board, laser diode, laser diode aligner, microscope objective (20X), microscope objective holder, xyz-translational stage, pin-hole masked photodetector connected to a multimeter, photodetector holder, rotation stage, two fiber chucks, two post bases and 3 posts, approximately 2 m length of a single-mode fiber, razor blade, fiber cutter, index matching liquid.

#### **Theory**

In single-mode fibers, it is the transverse distribution of the propagating mode rather than the core diameter and the numerical aperture that is important in estimating several propagation and the performance characteristics of these fibers. Thus *mode field diameter* (MFD), which is a measure of the transverse extent of the modal field distribution(i.e. of the  $LP_{01}$  mode), is an important parameter used to characterise a single-mode fiber. It is

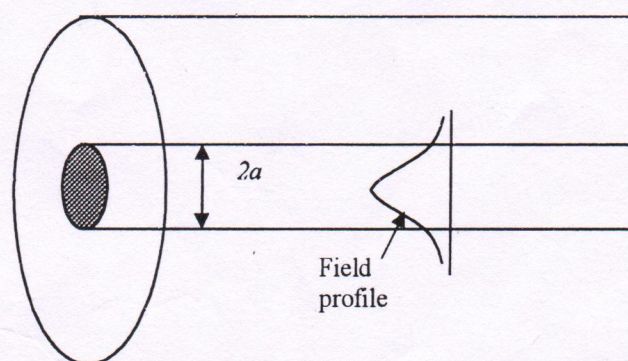


**Fig. 3.1 Schematic diagram of the amplitude distribution of the propagating fundamental mode in a single-mode fiber**

analogous to the core diameter in a multimode fiber, indicating the region of field confinement, and it also takes into account the wavelength dependent extent of penetration of the field into the fiber cladding. This parameter can be determined from the mode field distribution of the fundamental  $LP_{01}$  mode, which is shown in Fig. 3.1. It essentially specifies the transverse extent of this fundamental i.e.  $LP_{01}$  mode.

Knowledge of MFD is very useful in estimating joint loss between two single-mode fibers, coupling efficiency, cutoff wavelength, backscattering characteristics, microbending losses, and even waveguide dispersion.

For most single-mode optical fibers of the type used in communication systems, the near field of the fundamental mode can be well approximated by a Gaussian function of the form[3]:

$$\psi(r) = A \exp(-r^2 / w_0^2) \quad (3.1)$$

where  $A$  is a constant. The quantity  $2w_0$  gives the Gaussian MFD of the fiber; at the operating wavelength; usually,  $w_0 \approx a$ , where  $a$  is the core radius. Theoretically,  $w_0$  can be estimated by maximising the launching efficiency between a free space Gaussian optical field and the single-mode fiber [4]. Marcuse has shown that for a step-index single-mode fiber, the following empirical expression may be used to determine  $w_0$  [4]:

$$\frac{w_0}{a} \approx \left( 0.65 + \frac{1.619}{V^{3/2}} + \frac{2.879}{V^6} \right); \quad 0.8 < V < 2.5 \quad (3.2)$$

Since, the far-field of a diffracting field, which is actually the Fraunhofer diffraction pattern, is Fourier transform of its near field, it can be analytically shown that the far-field pattern of a Gaussian mode distribution[5] given by the above equation is again a Gaussian distribution and the corresponding intensity pattern is given by:

$$I(r, z) = \frac{I_0}{[1 + \gamma^2(z)]} \exp[-2r^2 / w^2(z)] \quad (3.3)$$

where  $w(z) = w_0 [1 + \gamma^2(z)]^{1/2}$  and  $\gamma(z) = \frac{\lambda z}{\pi w_0^2}$ .

Equation (3.3) represents the farfield intensity distribution. The parameter  $w(z)$  is the far-field mode field radius (MFR) of the Gaussian amplitude distribution. The far-field distribution refers to the angular dependence of the output field intensity, sufficiently far from the output end of the fiber. For practical purposes, if the distance  $z$  of the observation plane from the diffracting aperture is such that  $z \gg w_0^2 / \lambda$ , observation plane is said to be in the far-field. For such large values of  $z$

$$w(z) \approx \frac{\lambda z}{\pi w_0} \quad (3.4)$$

Accordingly, the Gaussian MFD ( $2w_0$ ) of a single-mode fiber can be easily obtained from a measurement of the angular distribution of its far-field measurements as discussed

below. Using Eq.(3.4), the far-field intensity distribution of a Gaussian field [Eq.(3.1)] is approximately given by[3],

$$\begin{aligned} I(r) &= B \exp \left[ -\frac{2\pi^2 r^2 w_0^2}{\lambda^2 z^2} \right] \\ &= B \exp \left[ -\frac{2\pi^2 w_0^2}{\lambda^2} \tan^2 \theta \right] \end{aligned} \quad (3.5)$$

where  $B$  is a constant independent of  $r$  and  $\tan \theta = r/z$ ,  $\theta$  being the far-field diffraction angle. The angle  $\theta_e$  at which the far-field intensity drops down by a factor of  $e^2$  from its maximum value at  $\theta = 0$  (see Fig. 3.2) would then be given by[2,3]:

$$\tan \theta_e = \frac{\lambda}{\pi w_0}$$

which yields

$$w_0 = \frac{\lambda}{\pi \tan \theta_e} \quad (3.6)$$

Thus, by measuring  $\theta_e$ , one can easily calculate the Gaussian mode-field diameter (MFD)  $2w_0$ .

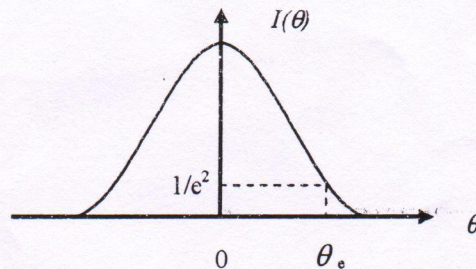


**Fig. 3.2 Determination of  $\theta_e$  from the measured angular distribution.**

### Procedure

Figure 3.3 shows the schematic of the set-up for the measurement of the mode field diameter of a single-mode fiber. For this, following procedures have to be followed step by step:

1. Mount the laser diode in the aligner and adjust with the help of the aligning screws.
2. Fiber ends are prepared so that it has well-cleaved ends. The cladding modes are removed by applying an index matching liquid (e.g. liquid paraffin) over a few centimeters of the bare fiber, near both the input and output ends and then clamped over the fiber chucks with the clamping magnets.
3. The output end of the fiber is clamped over a post base in such a way that the tip of the fiber is positioned on the axis of rotation of the rotational stage.

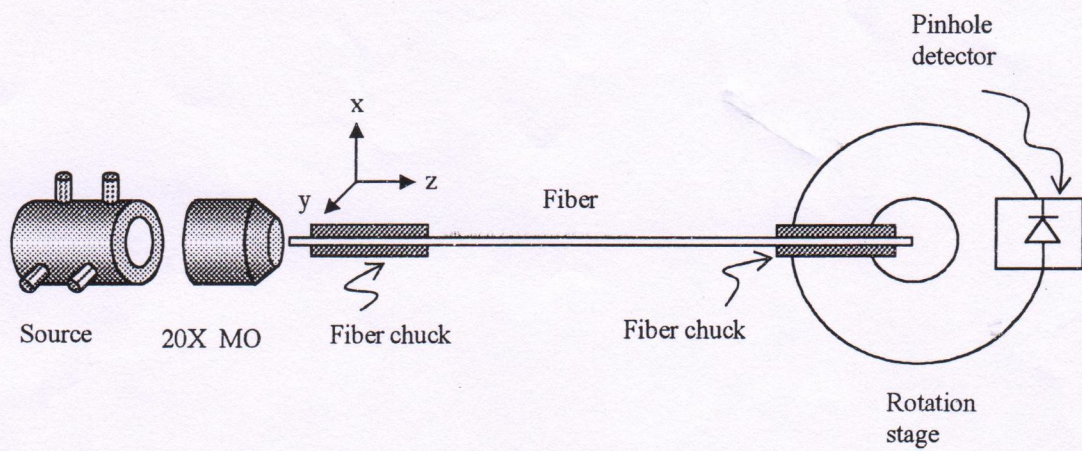


**Fig. 3.3 Experimental setup for scanning the far-field intensity distribution of a single-mode fiber**

4. Light is launched from the laser diode using a 20X microscope objective into the fiber.
5. A pinhole-masked photodetector is mounted on the rotational stage and the height of the fiber tip is so adjusted that the pinhole is positioned at the same horizontal level as the fiber end.
6. Now, without disturbing the input coupling, angular intensity distribution in the far-field (circular) spot of the fiber is scanned in suitable steps (say, in steps of  $0.5^\circ$ ), and for each recorded angular position the multimeter reading is recorded. The measured data will correspond to far-field angular intensity distribution.
7. Plot of the multimeter reading versus the angular position of the detector represents the recorded far-field intensity distribution. From this plot, calculate the value of the angle  $\theta_e$  at which the intensity is reduced to  $1/e^2$  of the maximum intensity (at  $\theta = 0$ ).
8. Using this angle, calculate the Gaussian mode field diameter ( $2w_0$ ) from Eq. (3.6).

### Observations:

Least count of the rotation stage =

S. No.	Reading on the rotation stage (in degrees)	Power meter reading ( $\mu\text{W}$ )

## **Result**

A typical variation of experimentally measured angular distribution of the far-field output power is shown in Fig.3.4, corresponding to a given single-mode fiber (Fibercore, SM600). In this figure, the filled squares show experimentally observed values, whereas the curve with circles shows the Gaussian fit to these experimental data. The horizontal line drawn in the plot shows the level at which the intensity drops down to  $1/e^2$  of the maximum output power. The line intersects with the plot at two angles, which can be directly read from this plot. From this plot,  $\theta_e$  (angle at which, the intensity drops down to  $1/e^2$  of its maximum value) comes out to be  $\approx 5.06^\circ$ . Using this value of  $\theta_e$  and the wavelength of the radiation emitted by laser (which is equal to 633nm), Eq. (3.6) yields Gaussian mode field diameter (MFD)  $\approx 4.5\mu\text{m}$ , which is in excellent agreement with the nominal value provided by the manufacturer, i.e.  $4.7\mu\text{m}$ .

Evaluation of MFD of SMF600; small pin hole

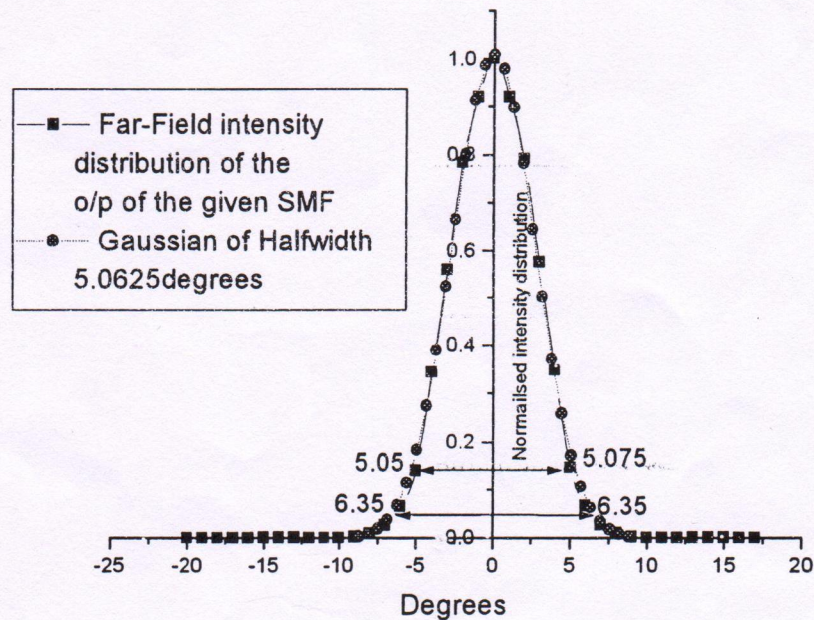


**Fig. 3.4 A typical plot of far-field intensity distribution of a single-mode fiber**

## **Comments**

It is necessary that the far-field intensity pattern be detected at a sufficiently large distance from the center of the fiber output end such that good angular resolution is achieved in detection. Furthermore, the angular sector scanned in front of the fiber must be sufficiently wide (between  $\pm 20^\circ$  and  $25^\circ$ ) to completely include the main lobe of the radiation pattern.

Although this method appears to be quite simple and straightforward, following points must be ensured at the time of performing the experiment:

1. The fiber end faces must be of good quality.
2. Cladding-mode strippers must be used.
3. The output end of the fiber must be positioned in such a way that the axis of the rotation of rotation stage passes through it.

The fiber used in this experiment was a Fibercore SM600, single-moded at 632.8 nm. If a single-mode fiber designed for operation at a given wavelength is operated at the longer wavelength, the modal field will spread more into the cladding of the fiber [3], thereby yielding a relatively larger mode field diameter.

Finally, it should be noted that the method described here for the measurement of mode field diameter is not unique, and several other methods have also been proposed [3]. Also note that in general the mode field varies with variation in the refractive index profile; Infact it can deviate substantially from a Gaussian distribution in case of complex fiber refractive index profiles ex. those encountered in specially dispersion shifted fibers like DSF, non-zero DSF (NZ-DSF) and dispersion compensating fibers(DCF).In such cases, most standard practice is to define the MFD of the fiber through the “Petermann MFD( $2w_p$ )”[3,6].

## References

1. A. K. Ghatak and M. R. Shenoy (Ed.), *Fiber Optics Through Experiment*, Viva Books Private Ltd., New Delhi (1994).
2. K. Thyagarajan, B. P. Pal and A. Kumar, “Characterization of Optical Fibers for Telecommunication and sensors-Part II: Single-mode Fibers”, *Int. J. of Optoelectronics*, vol. 3, p. 153 (1988).
3. A. Ghatak and K. Thyagarajan, *Introduction to Fiber Optics*, Cambridge University Press, Cambridge (1998).
4. D. Marcuse, “Loss analysis of single mode fiber splices”, *Bell Syst. Tech. J.*, vol. 56, p. 703 (1977).
5. A.K. Ghatak and K. Thyagarajan, *Optical Electronics*, Cambridge University Press, Cambridge (1989).
6. B.P. Pal, “Transmission Characteristics of Telecommunication Optical Fibers” in *Fundamentals of Fiber Optics in Telecommunication and Sensor Systems* by B.P. Pal (Ed.), New Age Publications, New Delhi (2002).

## **4. Refractive Index Profile of a Multimode Fiber**

---

### **Aim**

To measure the near-field intensity profile of a multimode fiber and hence its refractive index profile.

### **Apparatus**

Tungsten halogen lamp, assorted microscope objectives (20X, 40X), two XYZ translation stages, two V-groove fiber mounts, a pinhole detector mounted on a translation stage with an output cable for connecting to a power meter, index matching liquid for use as cladding mode stripper.

### **Theory**

The method essentially involves a scan of the near-field intensity distribution that exists at the output end of a short length (typically one to two meters) of multimode fiber, in which all possible guided modes are excited approximately equally by means of an incoherent Lambertian source<sup>1</sup>, such as a tungsten halogen lamp (or an LED). It can be shown that the power accepted at any point ' $r$ ' in the fiber core from a Lambertian source is directly proportional to square of the local numerical aperture. Evidently, the maximum power  $P_m$  that can be accepted by the fiber corresponds to the position  $r$  at which the NA is maximum. In an ideal fiber, this point would correspond to the fiber axis i.e.  $r = 0$ . However, many real fibers are characterized by an index dip at  $r = 0$  so that the maximum index  $n_m$  does not necessarily occur on the axis. In terms of the maximum power ( $P_m \equiv P(r = 0)$ ) that can be coupled into a fiber is given by [1].

$$\frac{P(r)}{P_m} = \frac{n^2(r) - n_{cl}^2}{n_m^2 - n_{cl}^2}. \quad (4.1)$$

For small refractive index differences,

$$\frac{P(r)}{P_m} \approx \frac{n(r) - n_{cl}}{n_m - n_{cl}} \quad (4.2)$$

If all the guided modes propagate in the fiber without any differential attenuation or mode conversion, which essentially implies that we consider a short piece of fiber which is relatively straight and devoid of any imperfections, then the same power distribution, which was launched at the input end will exist at the fiber's exit face. Therefore, if this near field is scanned by a small area photodetector, the detector output will yield the near-field power distribution of the fiber and hence RIP of the fiber as per Eq. (4.1). However, since the fiber core diameter is typically about  $50\mu m$ , it is difficult to directly scan the fiber's near-field with sufficient spatial resolution. In practice, therefore, one

obtains a magnified image (of a convenient size) of the fiber output end, and this image is scanned by a small area photodetector [1].

Telecommunication-grade multimode fibers are designed to follow the nominal refractive index distribution given by:

$$n(r) = n_m \left[ 1 - 2\Delta \left( \frac{r}{a} \right)^q \right]^{1/2}, \quad r < a$$

$$n(r) = n_m [1 - 2\Delta]^{1/2} = n_{cl}, \quad r \geq a \quad (4.3)$$

where  $n_m$  is the axial refractive index at  $r = 0$ ,  $a$  is the core radius and  $\Delta$  is the relative core-cladding index difference:

$$\Delta = \frac{n_m^2 - n_{cl}^2}{2n_m^2} \approx \frac{(n_m - n_{cl})}{n_m} \quad (4.4)$$

$q$  is the index exponent which defines the shape of the core RIP. For example,  $q = 1$  corresponds to a triangular core RIP,  $q = 2$  corresponds to the parabolic core RIP and  $q = \infty$  represents the step index profile (see Fig. 4.3).

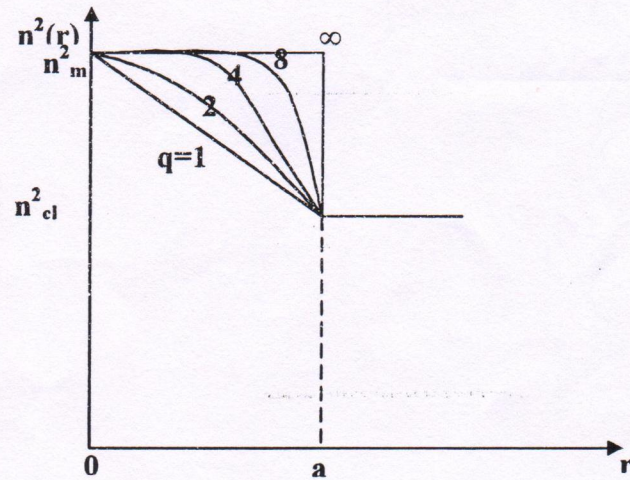


Fig. 4.1 Refractive index distributions of graded-core multimode fibers described by Eq.(4.3).

The so-called “optimum profile” corresponding to maximum transmission bandwidth occurs for  $q \approx 2$ . The exact value of  $q$ , in this case, is determined by the material composition of the fiber [2].

Using Eqs. (4.3) in Eq.(4.2) we get :

$$\frac{P(r)}{P(0)} = 1 - \left( \frac{r}{a} \right)^q \quad (4.5)$$

or

$$\log \left[ 1 - \frac{P(r)}{P(0)} \right] = q \log(r/a) \quad (4.6)$$

Hence, a log-log plot of  $[1 - P(r)/P(a)]$  against  $(r/a)$  will yield a straight line of slope  $q$  and hence the profile shape.

It can be seen from Eq. (4.2) that a measurement of the near field power distribution allows one to determine the refractive index difference  $[n^2(r) - n_{cl}^2]$  except for the unknown constant  $[n_m^2 - n_{cl}^2]$ . However,  $[n_m^2 - n_{cl}^2]$  is nothing but the square of the axial NA of the fiber that can be determined independently. Further, if the value of the cladding index  $n_{cl}$  is known (which for high-silica fibers may be taken to be approximately 1.46 in the visible wavelength region, corresponding to that of fused silica<sup>1</sup>), absolute values of the indices  $n(r)$  can be calculated from the measured near field power distribution.

## Experiment

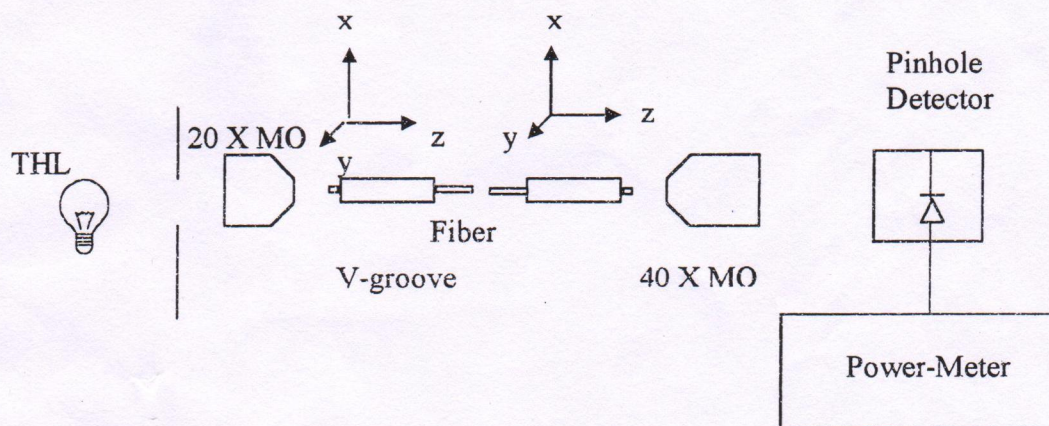


**Fig 4.2** Experimental set up for near -field measurement of a multimode fiber

## Procedure

The experimental set up is shown in Fig.4.2.

1. Light from a tungsten halogen lamp (THL), which is an incoherent source of light, is coupled into the given multimode fiber (about 1 metre long) by means of a 20X microscope objective (MO). The NA of the objective should be equal to or greater than the fiber NA in order to ensure excitation of all the guided modes. This launch optics is known to effectively approximate a Lambertian source.
2. The fiber ends are mounted on two XYZ-stacks. It is essential to have a good end-finish of the fiber ends by making good quality fiber cuts. Care must be taken to strip off the cladding modes by applying an index matching liquid, e.g. glycerin or

<sup>2</sup>At 1.3  $\mu\text{m}$ , refractive index of fused silica is about 1.444

liquid paraffin, over a few centimeters length of the bare fiber, near both the input and the output ends.

3. Using the 40X MO, a magnified image of the output end of the fiber is formed on the scanning plane of a pinhole detector. The pinhole diameter determines the spatial resolution of detection.
4. The detector is mounted on a translation stage in order to scan the image along a diameter of the circular spot of the magnified near field image.
5. To check that the near field image is indeed formed on the detector plane, the following procedure may be followed: For a given position of the detector, the fiber exit face is moved to and fro (using micropositioners) along the axis of the optical system, in front of the imaging microscope objective. The position of the fiber for which the smallest and sharpest image could be seen on a screen coinciding with the plane of the detector will ensure the formation of the near field image on the detector. This is easily understandable on the basis of the well-known lens equation:  $1/u + 1/v = 1/f$  where  $u$  and  $v$  are the object (in this case, fiber output end) and image distances respectively, and  $f$  the focal length of the imaging MO.
6. The detector output is connected to a power meter. The power meter readings can then be used to construct the near-field of the fiber by plotting power meter readings as a function of position of the detector.

Alternatively, if the detector is mounted on a motor driven translation stage or a scanner, the detector output could be directly fed to the Y-input of an XY-chart recorder. The near-field can then be obtained directly on the recorder as the 'X-arm' of the recorder is swept along the chart paper. The detector scanning speed and the sweep rate of the recorder should be chosen suitably to obtain a smooth record of the near-field profile.

### Observations:

Value of  $a$  from the graph =

S No.	Distance from the fiber axis, $r$ (a.u.)	Power Meter Reading ( $\mu\text{W}$ )	$\log(r/a)$	$\log[1 - P(r)/P(a)]$

## Results

The near field profile obtained as described above would be normally symmetric in shape about the central maxima (or minima, for fibers having a dip in the index profile) corresponding to  $r/a = 0$ . Since there is usually a rounding off at the core edge of the profile, it is difficult to precisely pinpoint the core-cladding interface on the measured near-field profile. This difficulty can be overcome by choosing the  $x$ -coordinate at which the near field intensity drops down by 95% from its maximum value as the reference for  $r/a = 1$  (see Fig 4.3). A plot of  $\log[1 - P(r)/P(a)]$  against  $\log(r/a)$  will yield a straight line with slope  $q$ , the index profile exponent.

In practice, it may be difficult to draw a single straight line connecting all the points due to the profile deviating from a perfect power-law distribution, and a mean value of  $q$  can only be obtained by estimating several localized  $q$  values corresponding to different small zones of the fiber core. Alternatively, a least square fit of Eq. (4.12) to the measured profile may be carried out to obtain the best-fitted value of  $q$ .

To determine the absolute values of refractive indices or the refractive index variation, we need to know the axial numerical aperture. The NA and hence  $\Delta$  can be estimated from a measurement of the fiber's far-field. The far-field can be measured by removing the imaging microscope objective from the near-field measurement set up and scanning the resultant output light from the fiber end. Thus, from a knowledge of  $n$  and  $\Delta$ , the measured near-field can be converted to a calibrated RIP by applying Eq. (4.11).

As a final check of the estimated profile, the experimentally obtained values of  $q$  and  $\Delta$  can be used in Eq. (4.3) and a comparison of the measured profile with that given by Eq.(4.3) can be made by plotting the latter also on the same graph.

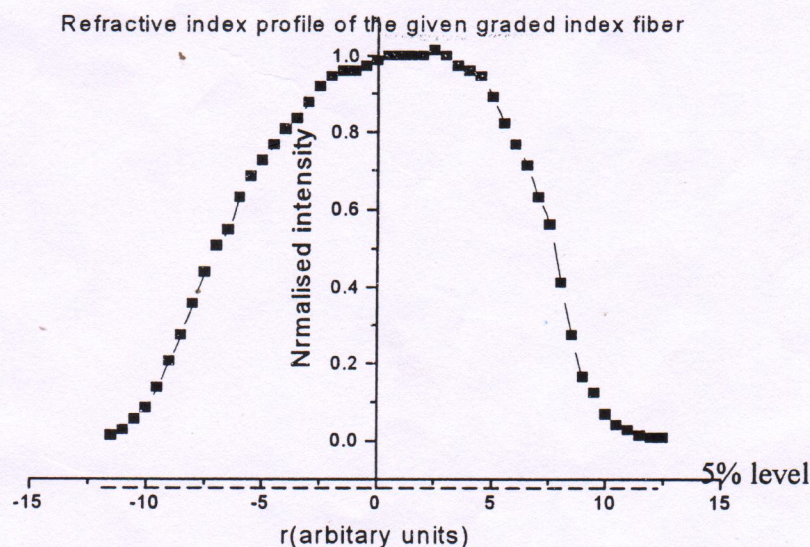


**Fig.4.3** Typical results of measurement of the near field of a graded-core multimode fiber

## Discussion

The most attractive feature of the method is that it provides a fast and relatively simple means to get a quick estimate of the core index profile and, for this reason alone, is employed by practically all fiber manufacturers. Nevertheless there is some controversy over the accuracy of the method. It is argued that since a relatively short fiber sample is excited in overfilled (both spatial and angular) launch conditions, the measured near field may include a significant contribution from leaky rays. One may then be required to take account of this by incorporating a correction factor [3,4] on the right-hand side of Eq.(4.2) in order to convert the measured near-field intensity profile to the fiber's refractive index profile. The presence of leaky rays leads to fiber length dependence of the measured near-field intensity distribution. This problem, however, is not as serious as it may seem because the leaky ray correction factors for a variety of profiles and fiber lengths were found to be almost identical up to a normalized radius  $r/a$  of 0.8, and differed by roughly  $\pm 6\%$  beyond  $r/a = 0.8$  up to  $r/a = 1$ . Thus, in practice for a quick general estimate of the RIP, one ignores the presence of any leaky rays in the measured near-field profile of the fiber.

Since, the derivation of Eq. (4.2) is based on the assumption that all modes carry equal amounts of power, care should be taken to avoid (i) any unnecessary stress at the fiber mounts and (ii) sharp bends along the length of the fiber sample. Care should also be taken to center the detector scan path on the fiber axis. Many laboratories use a vidicon with a monitor to scan the near-field. The near-field image of MCVD fibers is usually characterized by a dark central spot (corresponding to an axial index dip), which helps in defining the fiber center. This dark spot also helps the experimenter to check for optimal imaging of the fiber end-face on the detector plane by means of small adjustments in the ( $z$ - direction) position of the fiber end in front of the imaging objective so as to obtain maximum contrast in the near field pattern (NFP).

The inherent resolution afforded by the method is

$$\delta r \sim \frac{\lambda}{\pi(fiberNA)}. \quad (4.7)$$

For typical multimode fibers  $NA \approx 0.2$ ; with  $\lambda = 0.65$ , we get a maximum resolution of about  $1\mu m$ . On the other hand, detector spatial resolution is set by the size of the pinhole in front of it. If the fiber image size is  $l$  mm (diameter) at the detector plane and the pin-hole diameter is  $d$  mm, then the number of independent measurement points on the image plane is roughly  $l/d$ ; thus the resolution limit due to the pin-hole is  $Y = [2a/(l/d)]\mu m$ ,  $a$  being the core radius in  $\mu m$ . For high measurement precision,  $Y$  should be less than or of the order of the theoretical resolution given by Eq. (4.7); this can be achieved by having a relatively large image produced by a combination of a microscope objective and an eyepiece. However, in a graded-core fiber since the local fiber NA decreases from the core center towards the core-clad interface, there is a loss of resolution in the edges of the intensity profile; consequently, the core edges of the NFP are rounded (see Fig 4.3). Another point that may be noted while implementing this method is that the emission spectrum of the optical source must be sufficiently broad, or

the coherence length of the source should be very small, so that the finite numbers of guided modes do not interfere to produce a speckle pattern at the output end.

## **References**

1. F.M.E. Sladen, D.N. Payne and M.J. Adams, "Determination of optical fiber refractive index profiles by a near field scanning technique", *Applied Physics Letters*, vol.28, p. 255 (1976).
2. B.P. Pal (Ed.), *Fundamentals of Fiber Optics in Telecommunication and Sensor Systems*, Wiley Eastern, New Delhi (1992).
3. M.J. Adams, D.N. Payne and F.M.E. Sladen, "Correction factor for the determination of optical fiber refractive index profiles by NFS", *Electronics Letters*, vol.12, p.281 (1976).
4. D. Marcuse, *Principles of Optical Fiber Measurements*, Academic Press, New York (1981).
5. Ghatak A.K and Shenoy M.R, *Fiber Optics through Experiments*, Viva Books Ltd., New Delhi 1994.

## 5. Fiber-to-Fiber (Multimode) Splice Loss

---

### Aim

To measure the power loss at a splice between two multimode fibers, and study the variation of splice loss with transverse, longitudinal and angular offsets.

### Apparatus

Two XYZ-stacks, a rotation stage, tungsten halogen lamp/He-Ne laser, optical power meter, multimode fiber, V-grooves, etc.

### Theory

In any optical fiber telecommunication link, one or more splices/joints in the fiber cable is inevitable. The predominant method for connecting optical fibers involves a butt-joint connection. Any butt-joint requires three fundamental operations: fiber end preparation, fiber alignment to micron precision and alignment retention. Demountable connections retain alignment mechanically while permanent connections retain alignment through melting and fusing of the fiber ends in a fusion-splicing machine. In any fiber joint, the fiber ends must be prepared smooth and perpendicular to the fiber axis. The next step of aligning the fiber ends (to be jointed) is very crucial because any kind of misalignment would lead to a transmission loss. Loss at a fiber splice could originate from either or a combination of the following possible misalignments (see Fig. 5.1):

- i. Transverse offset between the fiber ends,
- ii. Angular tilt between the fiber ends,
- iii. Longitudinal end-separation between the fiber end faces.

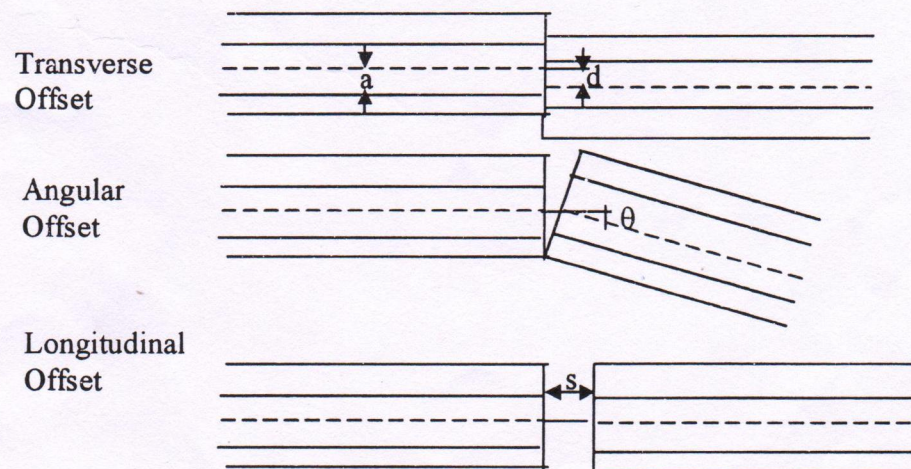


**Fig. 5.1** Three different types of offsets between the axes of the fibers at a splice-joint, which may lead to a transmission loss.

These fall under the category of extrinsic losses. In addition, either or a combination of the following may also result in a joint loss and these are sources of intrinsic loss:

- i. Reflection loss at the fiber-air interfaces.
- ii. Difference in characteristic parameters, e.g. refractive indices, index exponent; core dimensions, etc. between the two fibers.
- iii. Deformation of the end surfaces of fibers.

Major contributors to loss, however, at a splice are transverse offset, mismatches in core radii, and the relative core-cladding index difference (and hence NA).

An accurate model of splice loss is extremely difficult to construct. Losses at a fiber splice depend on various factors like mode power distributions, attenuation, and mode coupling characteristics of the fibers. These characteristics are difficult to measure experimentally and hence several approximate models have evolved in the literature to estimate splice losses in multimode fibers. Most successful attempt in this direction has been the phenomenological model of a Gaussian power distribution [1]. "This model gives a very good agreement with measured splice losses both for individual parameter mismatches and for combinations of both intrinsic and extrinsic mismatches that are extremely difficult to calculate any other way" [2]. In practice for a splice between two identical fibers, the following empirical but approximate expression for splice loss (in dB) due to transverse offset has been found to be accurate [2]:

$$\Gamma_d = -0.0001 + 0.6688 \left( \frac{d}{a} \right) + 4.136 \left( \frac{d}{a} \right)^2 + 0.5 \left( \frac{d}{a} \right)^3 \quad (5.1)$$

where  $d$  is the transverse effect (i.e. separation between the fiber axes) and  $a$  is the core radius of the fiber. It matches splice loss according to Gaussian model within 0.01 dB upto  $d/a = 0.8$ .

It has been observed that major contributors to splice loss namely, transverse offset, core radii- and  $\Delta$  mismatches between the transmitting and receiving fibers do not combine linearly. However, the following approximate relation may be used to model splice loss due to simultaneous presence of all the three factors [2]:

$$\Gamma = 2.0147 - 0.85k^2 - 1.035A + 5.4986 \left( \frac{d}{a} \right) \quad (5.2)$$

where  $A = \Delta_R / \Delta_T$  and  $k = a_R / a_T$ ; subscripts  $R$  and  $T$  refer to the receiving and the transmitting fibers; the parameter  $\Delta$  is defined as

$$\Delta \approx \frac{n_m - n_{cl}}{n_m}$$

where  $n_m$  and  $n_{cl}$  are the refractive indices of the core and cladding, respectively.

For angular offsets, transmission loss (in dB) may be approximately estimated from the following expression valid for step-index fibers [3,4]:

$$\Gamma_\theta = 10 \log_{10} \eta \quad (5.3)$$

$$\eta = \frac{16(n_1/n_2)^2}{[1 + (n_1/n_2)]^4} \left[ 1 - \frac{n\theta}{\pi n_1 (2\Delta)^{1/2}} \right] \quad (5.4)$$

where  $n_1$  is the core refractive index,  $n_2$  is the refractive index of the medium between the two fibers and  $\Delta$  is defined above. If the end-faces of two step-index fibers to be jointed are longitudinally separated by an amount  $s$ , transmission loss (in dB) can be approximately expressed as [5,6]

$$\Gamma_\theta = 10 \log_{10} \left[ 1 - \frac{s}{a} \frac{2}{\pi (NA)^2} \{ \sin^{-1}(NA) - NA \sqrt{1 - (NA)^2} \} \right] \text{ for } s/a \ll 1 \quad (5.5)$$

For parabolically graded-index fibers, corresponding expression is given by [5,6]:

$$\Gamma_s \approx 10 \log_{10} \left[ 1 - \frac{1}{2} (NA)(s/a) \right] \text{ for } s/a \ll 1 \quad (5.6)$$

We may note here that all the formulae [Eqs. (5.1)-(5.6)] are based on certain assumptions/models and care should be exercised while attempting any comparison of measurements with these theoretical expressions. *Fusion splicing* is the most widely used technique to permanently join two fibers. It is accomplished by localized heating (through an electric arc) of the interface between two butted and pre-aligned fiber ends. A high-voltage electric arc generated between two electrodes melts the fiber ends, and fuses them permanently as soon as the voltage is switched off. In the design of any such fiber fusion-splicing machine it is essential to have a prior knowledge of the factor that may lead to splice loss. In order to minimize splice loss, it is essential to understand relative affects of different local splice loss contributors. To appreciate it, the following experiment may be performed.

### Procedure

The experimental set up is shown in Fig. 5.2. Light from a tungsten halogen lamp is launched into a piece of multimode fiber. Cladding mode strippers should be applied at the input and exit ends of this fiber; henceforth this fiber will be referred to as transmitting fiber.

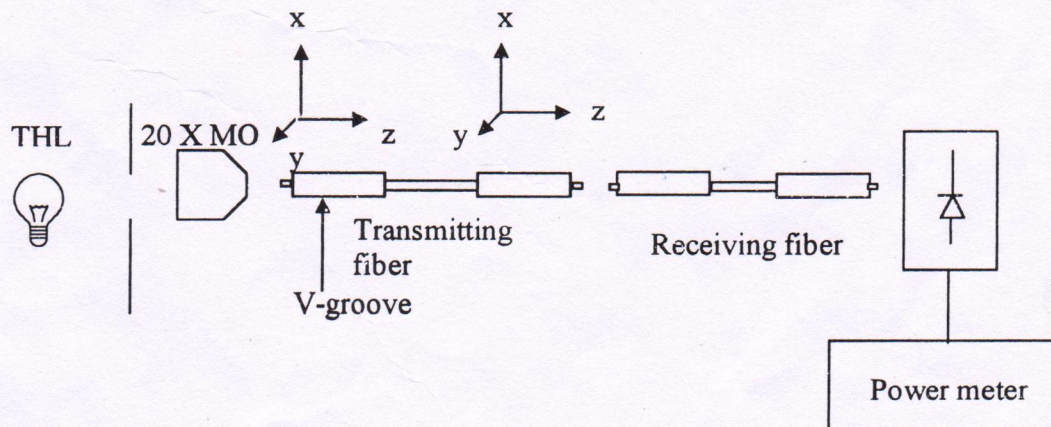


**Fig. 5.2. Experimental set up to measure fiber to fiber (Multimode) splice loss**

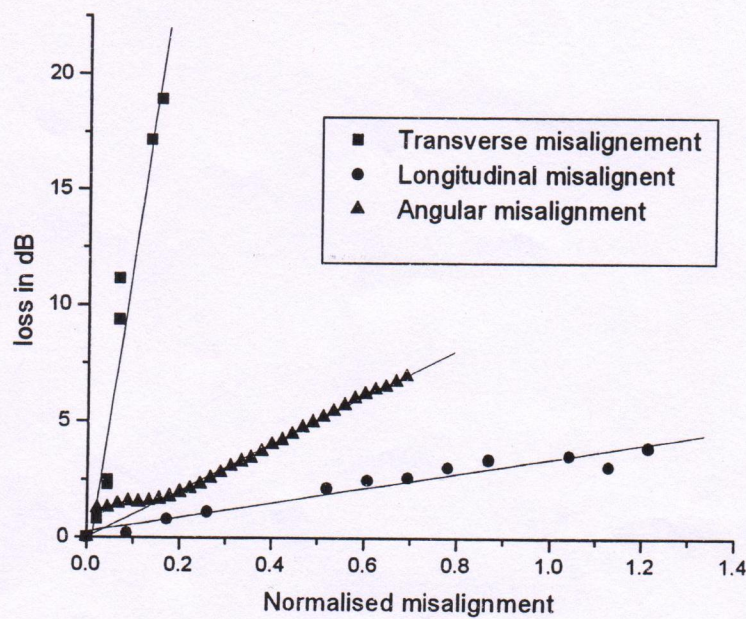


**Fig. 5.3** Typical results of splice losses due to various offsets between two multimode fibers.

A second piece of (preferably identical) multimode fiber, referred as the receiving fiber, is then brought near the output end of the transmitting fiber. Input end of the receiving fiber is mounted on a XYZ translation stage; the other end of this fiber is coupled to an optical power meter. One/two drops of cladding mode stripper is once again applied, as before, near the two ends of the receiving fiber. The XYZ translation stages are manipulated to induce any offset loss between the fibers. In actual practice for measuring transverse offset loss, it is recommended that the receiving fiber be moved away from the transmitting fiber (in the transverse direction) till the power meter reading reduces to almost zero (i.e. registers only ambient light). The receiving fiber's input end is then gradually moved into the field of view of the transmitting fiber to couple light from the transmitting fiber and the power meter reading is noted. The fiber could be moved in steps of one division of the graduated scale on the translation stage, and at each step the power meter reading is recorded. This procedure is continued till the receiving fiber once again gets out of the field of view of the transmitting fiber so that the power meter only registers background ambient light. The so tabulated readings of power meter versus linear position of the receiving fiber across the joint are then used to draw a graph between these two measurement parameters. Detected power can be further converted to a dB-scale by normalizing the power meter readings for each offset reading with the power meter reading for zero misalignment between the fibers, which would obviously correspond to the maximum of the power meter readings. In a similar manner, the measurements could be repeated for offsets in the two other orthogonal directions. If the fiber is perfectly circularly symmetric, then one of these two last measurements should yield results almost identical to the previous one. On the other hand, the third set of measurement, which would correspond to a longitudinal offset, the results would be quite

different compared to transverse offset. These measurements would reveal that longitudinal offset is more tolerable than transverse offset in terms of achieving a low loss fiber joint.

Tolerance to any angular offset on a plane between the fibers can likewise be obtained by mounting the input end of the receiving fiber at the center of a graduated turn table (i.e. fiber is initially aligned in the  $xy$  plane with a gap of  $2\text{-}3 \mu\text{m}$  (along  $z$ ) from the receiving fiber at the centre of the rotational stage. The output end of the transmitting fiber is mounted on a V-groove, which is freely suspended without contacting the rotational stage. Power coupled across the joint is then measured and recorded as a function of angular offsets. Angular offset is induced between the fiber ends by means of the rotational stage on which the receiving fiber is mounted. As before, care should be taken to use cladding mode strippers during the measurements.

## Observations

### 1) Transverse Misalignment:

Least count of micrometer screw =

Maximum power for zero misalignment =

S. No.	Micrometer reading ( $\mu\text{m}$ )	Power meter reading ( $\mu\text{W}$ )	Normalized power	Loss (dB)

### 2) Longitudinal Misalignment:

Least count of micrometer screw =

Maximum power for zero misalignment =

S. No.	Micrometer reading ( $\mu\text{m}$ )	Power meter reading ( $\mu\text{W}$ )	Normalized power	Loss (dB)

### 3) Angular Misalignment:

Least count of rotation stage =

Maximum power for zero misalignment =

S. No.	Reading on the rotation stage (degrees)	Power meter reading ( $\mu\text{W}$ )	Normalized power	Loss (dB)

## Results and Discussions

Make a comparative study of loss tolerance to various offsets between two fibers at a joint and highlight the ones that are most critical in the design of low loss fiber jointing machines. Some specimen results of splice loss measurements made on multimode fibers as a function of offsets are shown in Figure 5.3. It can be readily seen that splice loss is most sensitive to transverse misalignments. For a 20% off-set (relative to core diameter  $50 \mu\text{m}$ ), splice loss is about 0.4 dB. As already stated before, transverse off-set is the major contributor to splice loss and hence in the design of any splice machine one is required to take extreme care to avoid any potential source of transverse misalignment.

## References

1. C.M. Miller and S.C. Mettler, *Bell Syst. Tech. J.* 57, p.3167 (1978) and S.C. Mettler, *ibid*, vol.58, p. 2163 (1979).
2. C.M. Miller, S.C. Mettler, and F.A. White, *Optical Fiber Splices and Connectors: Theory and Methods*, Marcel Dekker Inc., New York (1986).
3. H.Tsuchiya, H. Nakagome, N. Shimizu and S. Ohara, "Double eccentric connectors for optical fibers", *Applied Optics*, vol.16, p.1323 (1977).
4. J.M. Senior, *Optical Fiber Communication: Principles and Practice*, Prentice-Hall International, London (1985).
5. W. Van Etten and J. Van Der Plaats, *Fundamentals of Optical Fiber Communications*, Prentice Hall International, Hempstead (1991).
6. W. Van Etten, W. Lambo and P. Simons, "Loss in multimode fiber connections with a gap", *Applied Optics*, vol.24, p.448 (1985).

## **6. Microbending Loss and Application in Sensing**

---

### **Aim**

To study a simple intensity modulated fiber optic pressure sensor based on microbending loss in a multimode fiber.

### **Apparatus**

Bread board, laser diode, laser diode aligner, microscope objective (20X), microscope objective holder, xyz-translational stage, photodetector with multimeter, photo-detector holder, rotation stage, microbend deformers, two fiber chucks, two post bases and 3 posts, weight box, about 2 m length of a multimode fiber, razor blade, fiber cutter, index matching liquid.

### **Theory**

To the majority of students “fiber optics” is synonymous with optical telecommunication. Another useful dimension of fiber optics is that it has also provided a revolutionary technology base for configuring a variety of optical sensors, which offer several advantages over existing traditional sensing techniques. Some of the key benefits are: immunity of several signals to electromagnetic interference, intrinsic safety in explosive

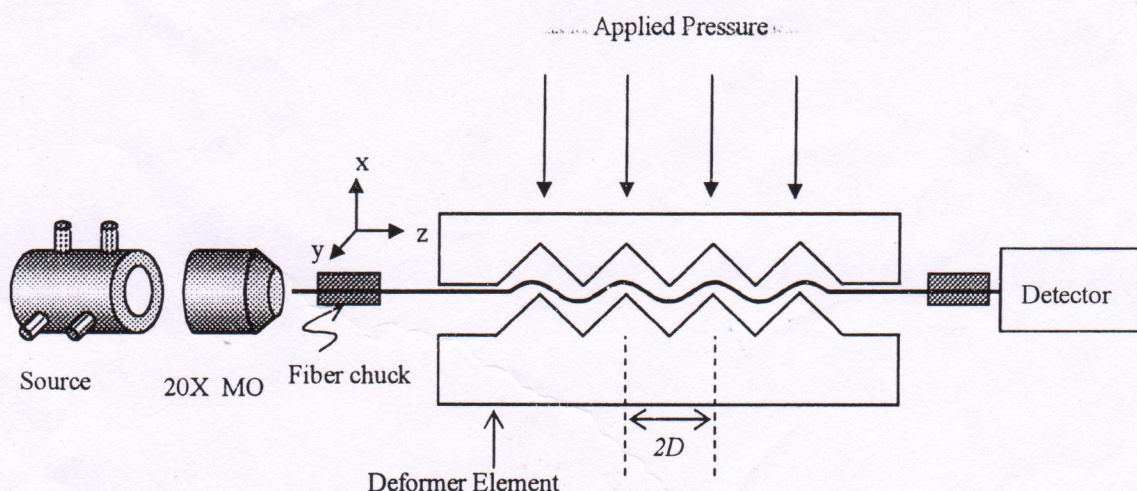


**Fig. 6.1(a)** Experimental set-up for a simple intensity modulated fiber optic pressure sensor using a multimode fiber

environments, offers remote sensing and distributed measurements, chemical inertness - thereby employable in chemical process and biomedical instrumentation due to their

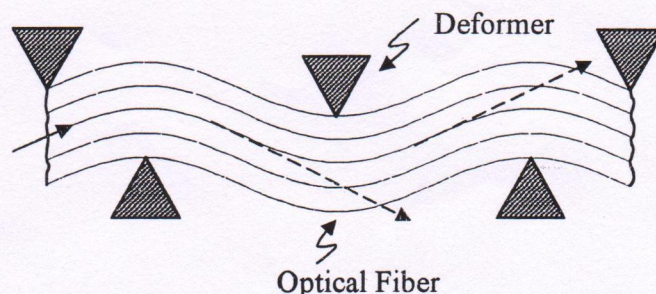


**Fig. 6.1 (b)** Principle of microbend induced attenuation in an optical fiber.

small size and mechanical flexibility. These advantages have led to intense R & D efforts around the world and development of a variety of fiber optic sensors for the measurement of pressure, temperature, liquid level, refractive index, pH, antibodies, electric current, displacement, rotation etc. Broadly, these sensors are classified either as *intrinsic* or *extrinsic* sensors. In an intrinsic sensor, one or more of the optical properties of the guided wave, such as intensity, phase, or state of polarization, is modulated by the measurand, which is then detected at the output. In contrast to this, in an extrinsic sensor, the fiber itself serves as a conduit to carry light signal to and from the sensor head/probe to be detected by a detector.

In this experiment, we describe a simple intrinsic fiber optic sensor based on the intensity modulation of light through a fiber by inducing microbends in the fiber through a periodic deformor element. When a portion of a fiber lay is sandwiched between two deformers and pressure is applied to one of these deformers, the fiber undergoes periodic deformation in the form of micro-bends (see Figure 6.1 (b)). The resultant mechanical deformation of the optical fiber perpendicular to its axis causes higher-order guided modes to radiate out of the fiber's core through the core-cladding interface as shown in the figure. This results in a drop of intensity of the transmitted light through the fiber with increasing deformation.

Figure 6.2 shows the basic geometry of the microbend element about one deformation point. As the pressure is applied (from the top) on the deformor, microbending occurs along the length of the fiber, and these bending results in loss of guided power by radiation at the bend. The loss in intensity for a bent fiber is given by [3]

$$\text{loss} = C \left( \frac{a}{R} \right)^2 \quad (6.1)$$

where  $R$  is the radius of curvature of the bend,  $a$  represents the fiber core radius and  $C$  is

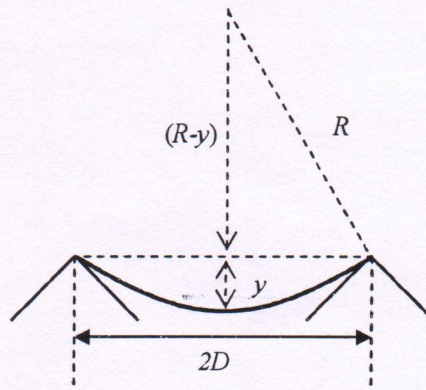


**Fig. 6.2 Geometry of the microbend**

a constant. Thus, for a given fiber the pressure applied can be related to the bend radius; which is given by (see Fig. 6.2)

$$R = \frac{(y^2 + D^2)}{2y} \quad (6.2)$$

where  $y$  is the displacement of the deformer element and  $2D$  is the distance between the contact points of the deformer element, which is equal to the pitch of the element. Thus, the transmittance  $T$  through the fiber is

$$\begin{aligned} T &= 1 - loss \\ &= 1 - \frac{Ca^2}{\left(\frac{y^2 + D^2}{2y}\right)^2} \\ &= 1 - C' \left( \frac{q}{1+q^2} \right)^2 \end{aligned} \quad (6.3)$$

where

$$C' = \frac{4Ca^2}{D^2} \quad (6.4)$$

and

$$q = \frac{y}{D} \quad (6.5)$$

The applied force and hence the pressure is proportional to the displacement  $y$ . Therefore in terms of pressure, we have

$$q = \frac{PA}{kD} \quad (6.6)$$

where  $P$  is the pressure,  $A$  is the surface area of the deformer and  $k$  is a constant.

## Procedure

Figure 6.1 shows the basic configuration of a fiber-optic microbend displacement sensor. For this, following procedures have to be followed step by step:

1. Mount the laser diode on the aligner and adjust with the help of the aligning screws.
2. Fiber ends are prepared so that it has well-cleaved ends, and clamped over the fiber chucks with magnets. One end of the fiber is fixed in the xyz-translational stage and other in post bases.
3. Light is launched from the laser diode using a 20X-microscope objective into the fiber (as discussed in Experiment no. 1). The output end of the fiber is coupled to the photodetector, connected to the multimeter to measure the amount of light transmitted through the fiber.
4. Microbend deformor is introduced somewhere along the length of the fiber as shown in the experimental set-up. By gently pressing on the deformor element, observe drop in the transmitted light intensity through the fiber.
5. Apply different pressure by placing suitable weights on the deformor, and each time note down the multimeter reading corresponding to the output of the detector.
6. Plot the measured relative output powers as a function of the applied weights.
7. Best fit the theoretical expression for transmittance ( $T$ ) (Eq. 6.3) vs. weight to the experimentally observed data by adjusting  $C'$  as the fitting parameter.

## Observations

Microbend period 1 = (mm)			Microbend period 2 = (mm)		
Mass (gm)	Detected Power ( $\mu\text{W}$ )	Normalized Power	Mass (gm)	Detected Power ( $\mu\text{W}$ )	Normalized Power

128.58 gm

## **Result:**

Figure 6.3 shows a graph of the measured light transmittance through a microbend modulated fiber-optic sensor versus the applied weight. The diameter of the fiber core was  $49 \mu\text{m}$  and numerical aperture was 0.19. In this figure, filled squares represent experimentally observed values and the solid curve is the least square fit to the data. As can be seen, the transmittance varies almost parabolically with the applied pressure. Figure 6.4 shows the corresponding variation with the primary jacket of the fiber removed. As expected, the latter case is more sensitive to the applied pressure.

## **Comments**

The microbending sensitivity of the sensing fiber must be maximized. One of the most important parameters in determining the microbending sensitivity is the periodicity of the fiber deformation. To understand this, one has to consider the mode coupling effects in fibers. From the theory of mode coupling it is well known that when a periodic microbend is induced along the fiber axis, light power is coupled between modes with longitudinal propagation constant  $\beta$  and  $\beta'$  satisfying [2, 4]

$$\beta - \beta' = \pm \frac{2\pi}{\Lambda} \quad (6.7)$$

where  $\Lambda$  is the mechanical wavelength of the periodic perturbation.

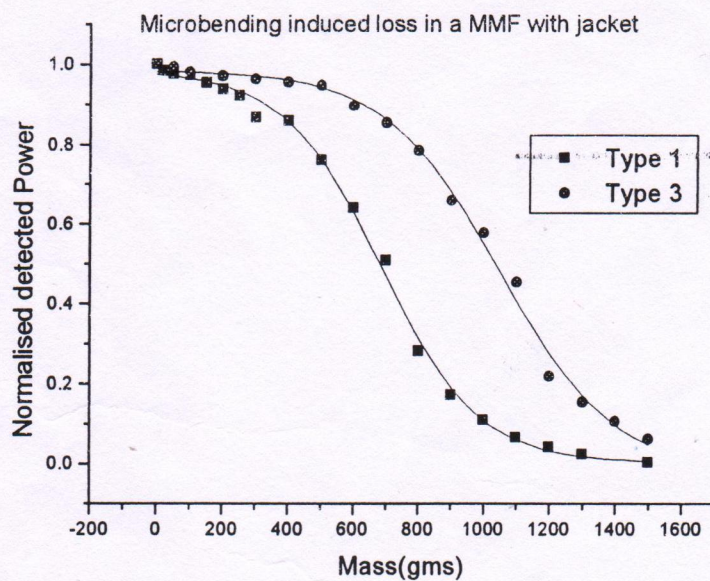


**Fig. 6.3** Amount of light transmitted through a microbend-modulated fiber-optic sensor versus the applied weight. The fiber core diameter and numerical aperture were  $49 \mu\text{m}$  and 0.19, respectively, and  $2D$  was equal to 1 mm. Here Type 1 corresponds to deformer 1 and Type 3 corresponds to deformer 3; the fiber was with its jacket in place.

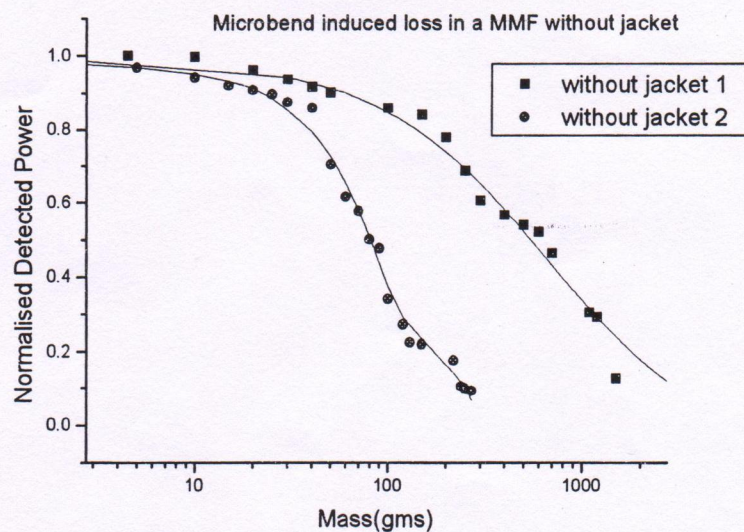


**Fig. 6.4** Amount of light transmitted through a microbend-modulated fiber-optic sensor versus the applied weight. The fiber core diameter and numerical aperture were  $49\mu\text{m}$  and 0.19, respectively, and  $2D$  was equal to 1 mm, except that the fiber is without the primary jacket.

For the fiber of given refractive index profile, the detail mathematical analysis predicts [5] that higher order modes can be coupled with small periodicity  $\Lambda$ , whereas lower order modes are coupled with large periodicity  $\Lambda$ . Microbending loss is caused by the coupling between guided modes and radiation modes. For small changes in the fiber deformation where neighboring mode coupling is believed to be valid, only adjacent modes are coupled. In this case microbending loss is due to coupling of the highest order guided mode to the first radiation mode. Such coupling can be realized with periodicities predicted by Eq. (6.7) [6], which significantly enhances the microbending loss and hence the sensitivity of the sensor.

In designing the microbend sensor it is important to consider the macrobending effect, i.e., light power loss caused by fiber deformations of the order of centimeters. Even though such macrobends cannot induce mode coupling (which requires small bends), they extend the field of the propagating modes into the coating, which in turn can introduce losses. In particular, macrobending removes the preferred higher order core modes, which are responsible for the microbending sensitivity. Therefore macrobending can significantly decrease the microbending effect and must be avoided by keeping the sensing fiber straight.

In designing the sensor, the length of the sensing fiber is an important parameter, which influences the sensitivity of the sensor. It has been found that the microbending sensitivity varies approximately linearly with the length of the sensing fiber [6].

For obtaining the best sensor response, following points must be realized, in addition, at the time of performing the experiment:

1. The fiber end faces must be of good quality.
2. Cladding-mode strippers must be used.
3. The two plates of the deformers must be accurately aligned.

The sensor response is critically dependent on the excitation conditions. To ensure that all the guided modes are excited in the multimode fiber, an overfill launch is applied at the input end of the fiber i.e. one uses a microscope objective of NA higher than that of the fiber for launching light into the fiber.

## References

1. B. Culshaw, *Fiber Optic Sensors and Signal Processing*, Peter Peregrinus, Stevenage (1984).
2. B. P. Pal (Ed.), *Fundamentals of Fiber Optics in Telecommunication and Sensor Systems*, Wiley Eastern Ltd., New Delhi (1992).
3. C. K. Kao, *Optical Fiber Systems: Technology, Design and Applications*, McGraw-Hill, New York (1982).
4. A. K. Ghatak and K. Thyagarajan, *Introduction to Fiber Optics*, Cambridge University Press, Cambridge (1998).
5. C. N. Kurtz and W. Streifer, *IEEE Trans. Microwave Theory Tech. MTT*, vol. 17, p. 250 (1969).
6. N. Lagakos, J. H. Cole, and J. A. Bucaro, "Microbend fiber-optic sensor", *Applied Optics*, vol. 26, p. 2171 (1987).

## 7. Bend-Induced Loss in a Single-Mode Fiber

---

### Aim

To study bend-induced loss in a single-mode fiber

### Apparatus

Bread board, laser diode, laser diode aligner, microscope objective (20X), microscope objective holder, xyz-translational stage, photodetector with multimeter, photo-detector holder, two fiber chucks, two post bases and 3 posts, a single-mode fiber (approx. 3m length), brass rods with circular cross section of different diameters (say, from 0.8 cm to 4 cm), razor blade, scotch tape, fiber cutter and index matching liquid.

### Theory

Radiative losses occur whenever an optical fiber is subjected to extrinsic perturbations like bend of a finite radius of curvature [1-6], and such losses are called *bend loss*. An optical fiber can be subjected to two types of bends: (a) random microscopic bends of the fiber axis, for example, those that may occur when a fiber is sandwiched between two sand-papers, and (b) macroscopic bends having radii that are large compared to the fiber diameter, for example, those that may occur during cabling and laying of the fiber cable, respectively. Here, we are mainly concerned with the power radiated from single-mode fibers due to the latter type of bending, which is sometimes referred to as *macrobending*. Any simple experiment that involves launching a laser light (e.g. from a laser diode) into a fiber that is first laid straight and then bent into an arc of a circle, would reveal that the fiber suffers radiation loss from the side at bends/curves along its path, which can be measured by measuring the drop in transmitted power with an optical power meter placed at the output end of the fiber - once laid straight, and then after introducing a bend in its lay.

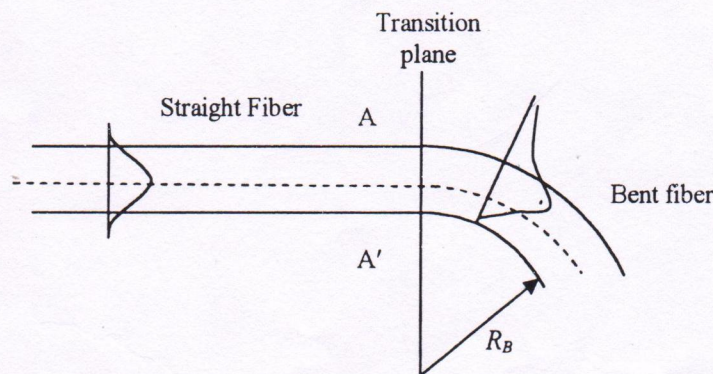


**Fig. 7.1** A qualitative representation of the shift in the Gaussian-like fundamental mode away from the fiber axis at a bend.

For relatively small bends, this loss is extremely small and is essentially unobservable. As the radius of curvature decreases, transmission loss increases exponentially until at a certain critical radius of curvature when the loss becomes observable. If the bend radius is reduced below this threshold point, the loss suddenly becomes extremely large.

We first look at the physical process involved in the bending loss. A bend can be treated as a straight section of the fiber joined to a curved section of the fiber and joined again to another straight section, as shown in Fig. 7.1. According to the ray analysis, there are no truly bound rays in a bent optical fiber. Thus, every ray is leaky and radiates power through the mechanism of tunneling or refraction. For example, the *meridional rays* in a bent fiber are either tunneling rays or refracting rays, and *skew rays* lose power at successive reflections either through tunneling or refraction.

Qualitatively, the bending loss can be explained by examining the modal electric field distribution as shown in Figs. 7.1 and 7.2. The bending loss can be accounted for by the *transition losses* and the *macrobend losses*. Transition loss is due to the abrupt changes in curvature occurring, e.g., at the cross sectional plane AA' of the fiber shown in Fig. 7.1. The predominant effect of curvature on the fundamental mode is to shift the peak of the field distribution radially outwards (in the plane of the bend) by a distance  $r_d$  from the fiber axis as shown in Fig. 7.1. This shift, which is rather difficult to obtain exactly, within the Gaussian approximation of the field, is given as [2]

$$r_d = \frac{\beta^2 w_0^4}{2R_c} \quad (7.1)$$

where  $\beta$  is the propagation constant of the mode in the straight fiber,  $R_c$  is radius of

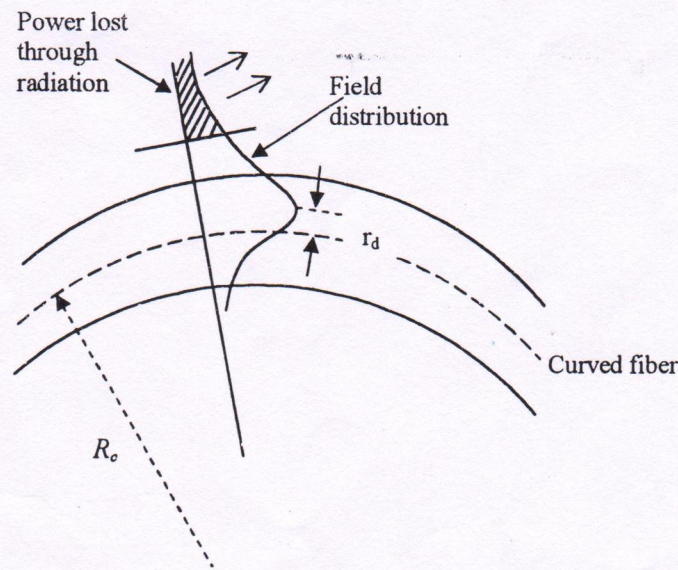


**Fig. 7.2** Schematic representation of the bending loss in a section of fiber bent into an arc of radius  $R_c$ .

curvature of the bend and  $w_0$  is the Gaussian spot-size [6]. Thus the transition loss is due to the mismatch over the plane AA' between the fields of the straight section and the offset field of the curved section.

To get a feel for the numbers involved, let us consider a typical SMF with  $n_1 = 1.46$ ,  $n_2 = 1.457$  at an operating wavelength ( $\lambda_0$ ) of 649 nm, and core radius  $a = 2.1 \mu\text{m}$ . which yields  $V \approx 1.90$ . The corresponding Gaussian spot-size is calculated using the empirical relation [6]

$$w_0 = a \left( 0.65 + \frac{1.619}{V^{3/2}} + \frac{2.879}{V^6} \right)$$

For the above SMF,  $w_0 = 2.791 \mu\text{m}$ . If we further assume that  $\beta \approx \frac{2\pi}{\lambda_0} \left( \frac{n_1 + n_2}{2} \right)$ , then for

$R_c = 0.5 \text{ cm}$ , one gets  $r_d = 1.206 \mu\text{m}$ . The transition loss is given by [6]

$$\alpha_t(\text{dB}) = 4.34 \left( \frac{r_d}{w_0} \right)^2,$$

and the corresponding transition loss turns out to be 0.81 dB.

The second mechanism of loss is the actual transmission loss suffered due to radiation from side of the bent fiber. We know that any bound (core) mode has an evanescent tail in the cladding, which decays almost exponentially with distance from the core-cladding interface [6]. Since the evanescent tail moves along with the field in the core, part of the energy of a propagating mode travels in the fiber cladding. In a straight fiber of arbitrary profile, the modal field at every point in the cross-section propagates parallel to the fiber axis with the same phase velocity, so that the planes of constant phase are orthogonal to the axis. However, if the fiber is bent into a planar arc of constant radius, as shown in Fig. 7.2, it can be intuitively seen that the fields and phase fronts rotate about the center of curvature of the bend with constant angular velocity. Consequently, the phase velocity parallel to the fiber axis must increase linearly with the distance from the center of the curvature of the bend. Thus, the evanescent tail on the far side of the center of curvature must move faster to keep up with the field in the core. At a certain critical distance  $d_c$  from the center of the fiber, the portion of the evanescent tail (in the cladding) would have to move faster than the speed of light in the fiber cladding to keep up with the core field. Since this is not possible as per fundamental laws of nature namely constancy of light's speed in a given medium, the optical energy in the evanescent tail beyond  $d_c$  radiates away [3]. Close to and within the core, the fields are accurately described by a local mode, provided the radius of curvature is sufficiently large.

The pure bend loss coefficient (in dB per unit length of the bent fiber) in a single moded step index fiber is given by [1]:

$$\alpha \approx 4.34 \left( \frac{\pi}{4aR_c} \right)^{\frac{1}{2}} \left( \frac{U}{VK_1(W)} \right)^2 \frac{1}{W^{3/2}} \exp \left[ -\frac{4}{3} \frac{R_c}{a} \frac{W^3 \Delta}{V^2} \right] \quad (7.2)$$

where,  $a$  is the core radius of the fiber,  $R_c$  is the radius of curvature of the bent fiber,  $K_1(x)$  is the modified Bessel function of second kind. The parameters  $U$ ,  $W$ ,  $V$  and  $\Delta$  are defined through:

$$U = a\sqrt{k_0^2 n_1^2 - \beta^2}$$

$$W = a\sqrt{\beta^2 - k_0^2 n_2^2}$$

$$V^2 = U^2 + W^2$$

$$\Delta \equiv (n_1 - n_2)/n_2$$

and

$$k_0 = 2\pi/\lambda_0$$

It should be noted that in evaluating the above expression, the quantities  $\lambda_0$ ,  $a$  and  $R_c$  must have the same units, e.g., centimeters (cm). For the fiber parameters considered above, one gets  $V \approx 1.90$ ,  $U \approx 1.49$ ,  $W \approx 1.18$ ,  $K_1(W) = 0.45$ , which yields  $\alpha = 51.52$  dB/cm when  $R_c = 0.5$  cm. One can also calculate the transition loss, which is usually much smaller than the pure bend loss.

In the experiment, a few turns are given to the fiber so that the loss is measurable and then  $\alpha$  is calculated as follows:

$$\alpha = -\frac{10}{L} \log \frac{P_2}{P_1} \quad (7.3)$$

where  $L$  is the length of the fiber (within the bend) i.e.  $2\pi R \times (\text{no. of turns})$ ,  $P_1$  is the output power without the bend in the fiber and  $P_2$  is the output power with the bend in the fiber.

## Procedure

Figure 7.3 shows the schematic of the set-up for the measurement of the macrobending loss in a single-mode fiber. For this, following procedures have to be followed step by step:

1. Mount the laser diode in the aligner and adjust with the help of the aligning screws.
2. Ends of a single-mode fiber of approximately 3m in length are prepared so that it has well-cleaved ends.
3. The cladding modes are removed by applying an index matching liquid (e.g. liquid paraffin) over a few centimeters of the bare fiber, near both the input and output ends and then clamped over the fiber chucks/holders. One end of the fiber is held in the xyz-translational stage and the other in a V-groove that is mounted on a post base.

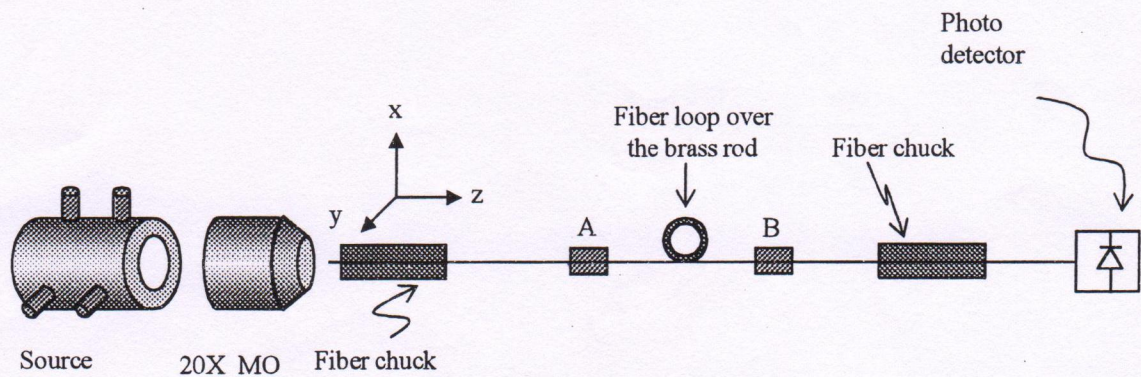


**Fig. 7.3 Experimental setup to study the macrobending loss in a single mode fiber**

4. Light is launched from the laser diode using a 20X-microscope objective into the fiber.
5. The output end of the fiber is coupled to the photodetector, connected to the multimeter to measure the amount of light transmitted through the fiber. The multimeter reading is then noted down. This is  $P_1$ , power without the bending around the brass/ aluminum rod. Now to measure  $P_2$ , i.e. the output power with the bending around the brass rod, following steps have to be carefully followed:
6. Fiber is clamped with cello tape at a distance 1 m from the input end (as shown in Fig. 7.3 at A) as well as just before the output end as (shown in Fig. 7.3 at B). In this way we would be having approximately 2 m length of the fiber in between the clamped point A and B.
7. Exactly between the clamped points, a smooth brass/aluminum rod of uniform cross section is fixed as shown in the set up and fiber is wound over it. For the brass rods of diameters between 2 to 4 cm, 10 to 20 turns (or more, to achieve significant difference between  $P_1$  and  $P_2$ ) of the fiber are wound on the rod. Whereas, for the brass rods having diameters from 1 to 2 cm, you may choose suitable number of turns between 1 and 10. Between A and B, the fiber segments on the either side of the rod should be stretched straight, bearing the same tension.
8. Vary the bending loss by changing the rods of different diameter and winding the fiber with suitable number of turns over it. Each time, note down the multimeter reading corresponding to the output of the detector.
7. Calculate the losses in dB per unit length using Eq. 7.3 and plot the measured loss as a function of the bending radius.

### Macrobending loss in Single Mode Fiber

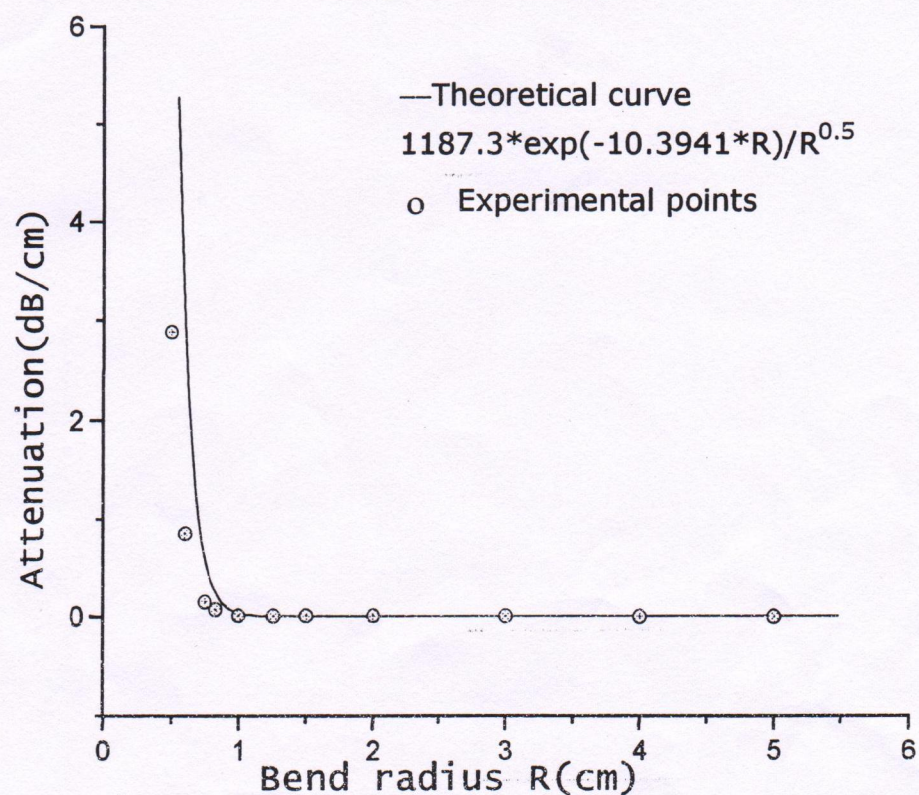


**Fig. 7.4** Bend loss of a single mode step-index fiber as a function of bend radius. The fiber core diameter  $\approx 4.2 \mu m$ ,  $\Delta \approx 0.002$  and  $V \approx 2.31$  at  $0.633 \mu m$ ; points represents to the measured data and the continuous curve represents the theoretical curve, obtained using Eqs.(2) and (3).

### Observations

Input power without any bend =

S.No.	Radius of the rod, $R$	No. of turns	Total length of the bent fiber, $L$	Output power	Power loss (dB)	Absorption coefficient ( $\alpha$ )

## Result

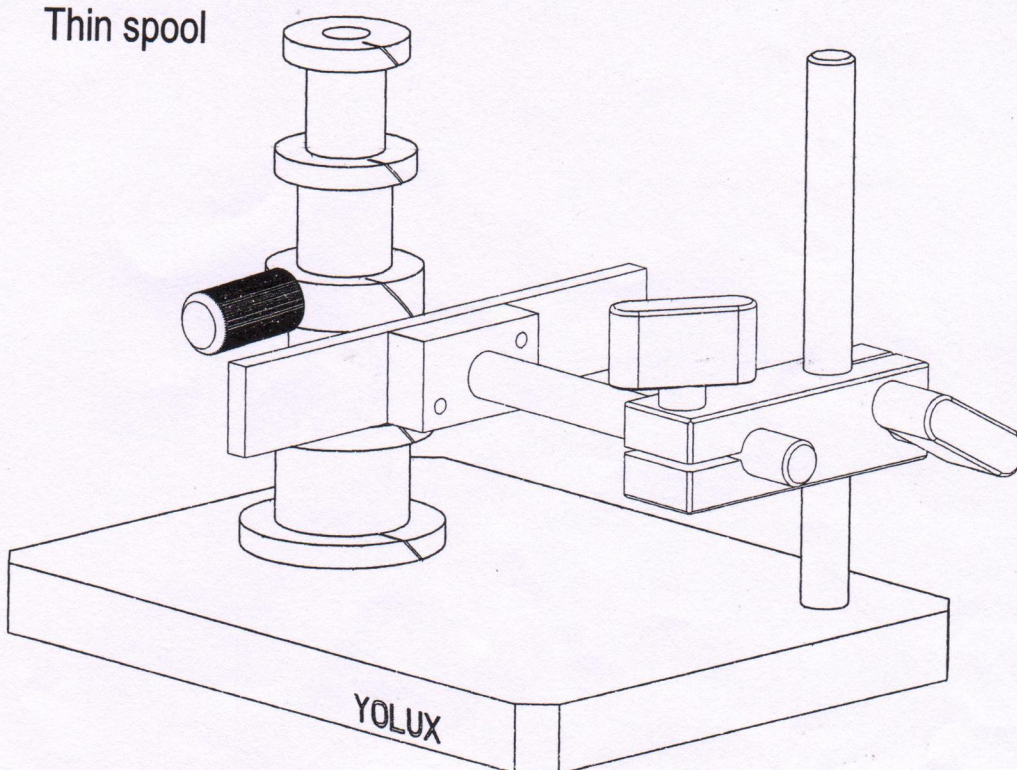
A typical variation of experimentally observed bend loss per unit length for a single-mode fiber (Fibercore, SM600) is shown in Fig. 7.4. The single-mode step-index fiber used for the experiment was having a nominal core diameter  $\approx 4.2 \mu\text{m}$ ,  $\Delta \approx 0.002$ ,  $V \approx 2.31$  at the He-Ne laser wavelength ( $0.633 \mu\text{m}$ ). In this figure, the filled circles show experimentally observed values, whereas the continuous curve shows the best fit to these experimental data. The experimental data usually starts deviating from the theoretical plot (obtained using Eq. 7.3), which may be because of not taking into account the transition loss. The procedure followed above for the bending loss measurement would not be suitable for multimode fibers since the bending loss per unit length in the fiber will be length dependent.

## References

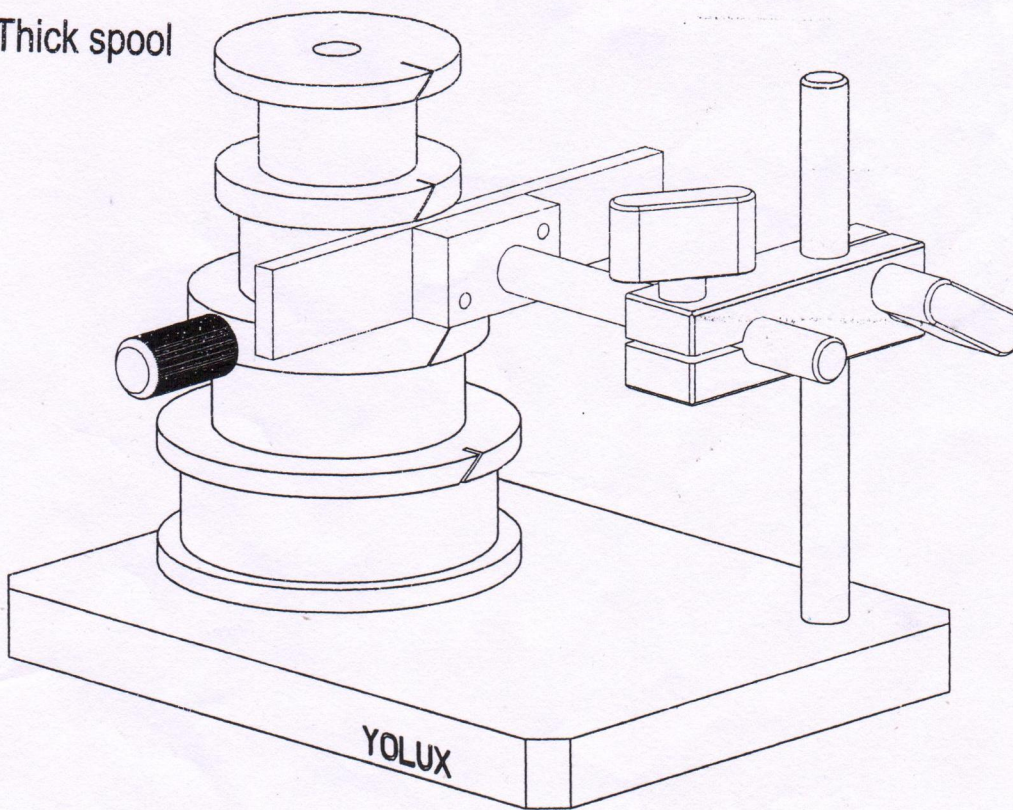
1. A. W. Snyder and J. D. Love, *Optical Waveguide Theory*, Chapman and Hall, London, (1983).
2. W. A. Gambling and H. Matsumura, *Trans. IECE Japan E* 61, p. 196 (1978).
3. D. Marcuse, "Curvature loss formula for optical fibers", *J. Opt. Soc. Amer.*, vol. 23, p. 216 (1976).
4. D. Gloge, "Bending loss in multimode fibers with graded and ungraded core index", *Appl. Opt.*, vol. 11, p. 2506 (1972).
5. S. J. Garth, "Fields in bent single-mode fiber", *Electron. Lett.*, vol. 23, p. 373 (1987).
6. See, e.g., A. K. Ghatak and K. Thyagarajan, *Introduction to Fiber Optics*, Cambridge University Press, Cambridge (1998).

Multi Spool Kit For Bend Loss Induced

Thin spool



Thick spool

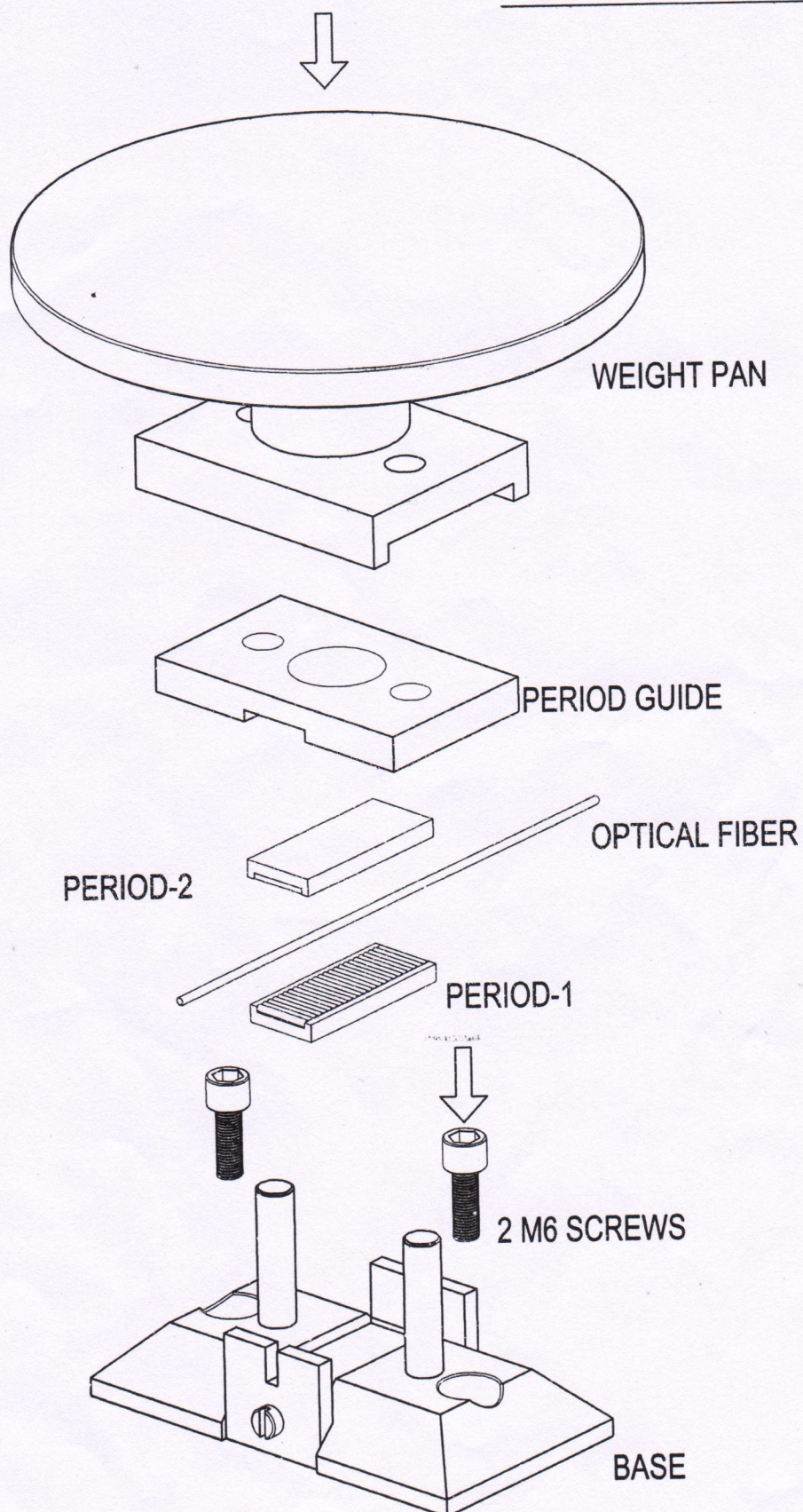


PLEASE CALL US FOR ANY FURTHER SPECIFICATION or CUSTOM DESIGN.



bipin behari dey & co Email: [yolux@rediffmail.com](mailto:yolux@rediffmail.com)  
Phone: +91 674 258 0056 Fax: +91 674 258 3895

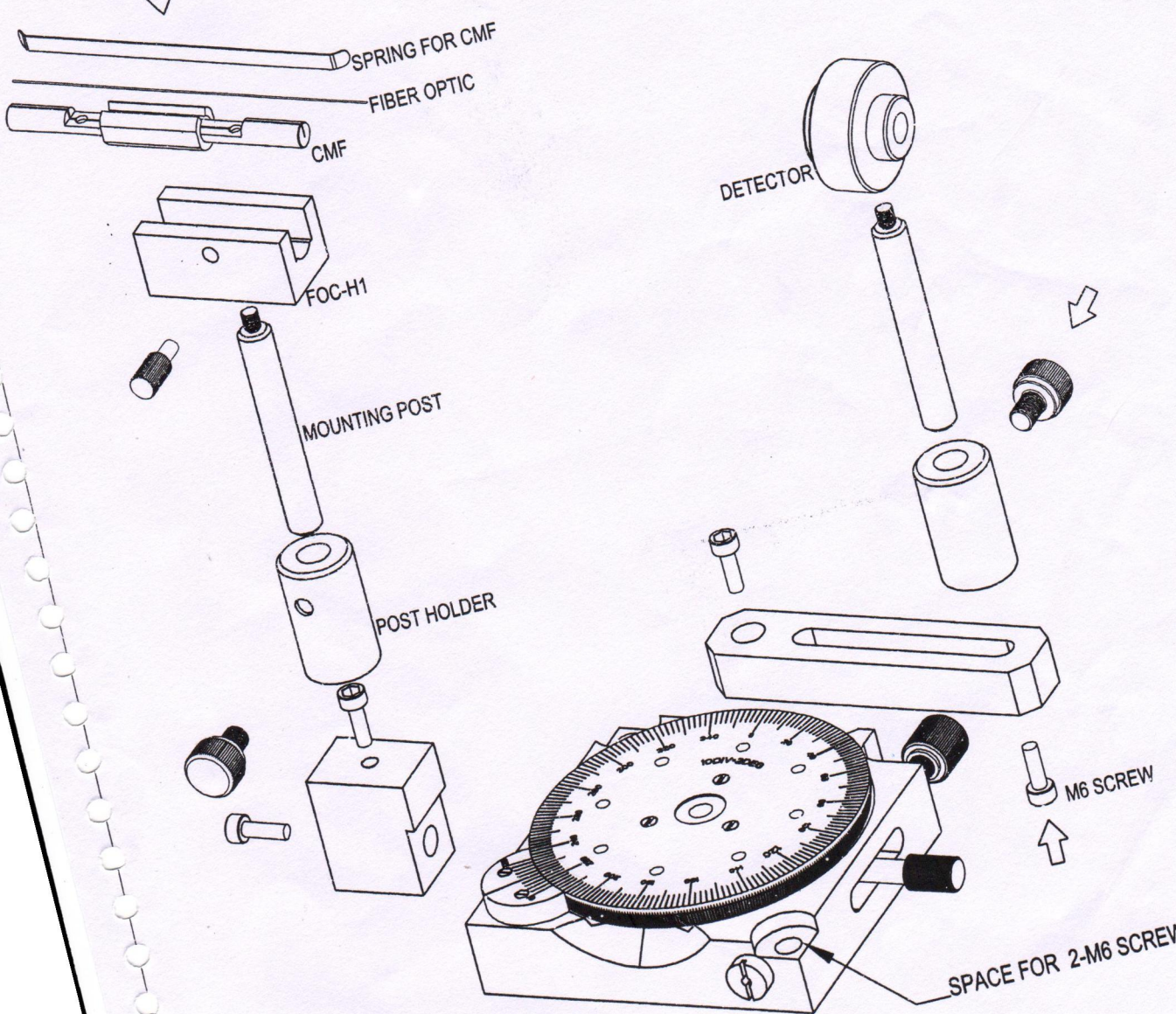
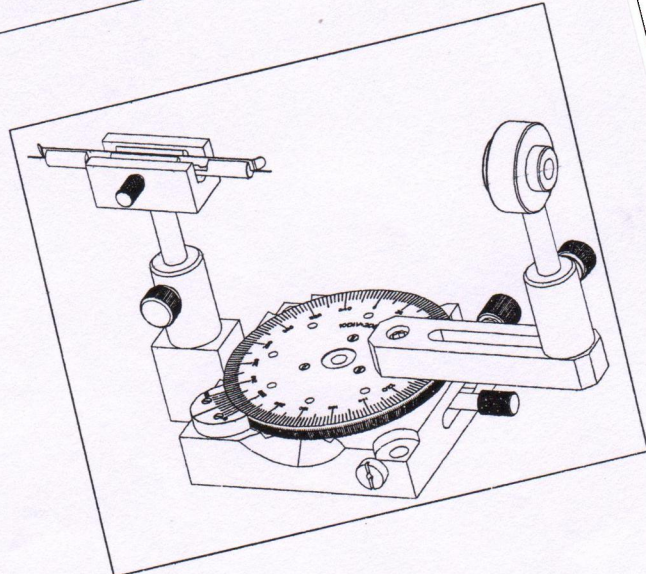
## MICROBENDING APPARATUS



PLEASE CALL US FOR ANY FURTHER SPECIFICATION or CUSTOM DESIGN.

SET UP OF RB-85 WITH FOC-H1

YOLUX  
FIBER OPTICS EDUCATION



PLEASE CALL US FOR ANY FURTHER SPECIFICATION or CUSTOM DESIGN.



bipin behari dey & co Email: yolux@rediffmail.com  
Phone: +91 674 258 0056 Fax: +91 674 258 3895

